Data supplement for Fonzo et al., Selective Effects of Psychotherapy on Frontopolar Cortical Function in PTSD. Am J Psychiatry (doi: 10.1176/appi.ajp.2017.16091073)

Supplemental Methods

Note: The text contained within the following sections is also reproduced in a companion publication in the same sample of participants (1): Participants and Assessments, General Inclusion and Exclusion Criteria, Behavioral Paradigms, MRI Data Acquisition, Randomization, Treatment Frequency and Length, *Therapist Competency and Supervision in Prolonged Exposure, Treatment Structure, Post-Treatment Clinical Assessment, and Functional Image Preprocessing.*

Participants and Assessments

Individuals, age 18-60, were recruited via advertisement for participation in a psychotherapy treatment study for survivors of trauma. After receiving a full explanation of study procedures, participants provided written informed consent for study participation. Trained PhD-level clinicians established DSM-IV diagnoses using the Clinician-Administered PTSD Scale for PTSD (CAPS)(2) and the Structured Clinical Interview for DSM-IV Diagnosis for non-PTSD diagnoses (SCID-IV)(3). IQ was estimated using the Wechsler Abbreviated Scale of Intelligence (WASI)(4). Additional secondary outcome measures included the Beck Depression Inventory-II (BDI-II)(5), a 21-item self-report inventory of depressive symptoms in which each item is rated on a 0 to 3 scale of severity. Scores range from 0 to 63. Participants provided self-report measures of PTSD symptoms using the PTSD Checklist Civilian version for DSM-IV (PCL-C)(6), a 17-item self-report measure in which PTSD symptoms are rated on a 1 to 5 scale of severity. Total scores for this measure range from 17 to 85. Quality of life was assessed using the WHO Quality of Life BREF Scale (WHO-QoL)(7), a 26 item self-

report inventory of four domains of quality of life: physical health, psychological health, social relationships, and environment. Each domain is scored on a scale ranging from 4 to 20, with higher numbers indicating better quality of life in that domain. Additionally, participants completed self-report measures of emotion regulation difficulties and style. These included the Emotion Regulation Questionnaire (ERQ)(8), a 10 item self-report measure that asks participants to rate the tendency with which they regulate and manage emotions on a 7 point Likert scale. There are two subscales, one measuring the tendency to engage in Cognitive Reappraisal and the other measuring the tendency to engage in Expressive Suppression. Scores reflect the average rating for each subscale and range from 1-7. Additionally, participants completed the Difficulties with Emotion Regulation Scale (DERS)(9), a 36 item self-report measure designed to assess multiple aspects of emotional dysregulation. Items are scored on a 5 point scale indicating the frequency with which an individual experiences a specific type of difficulty in the regulation or experience of emotion. There are six subscales: 1) Nonacceptance of Emotional Responses; 2) Difficulties Engaging in Goal-Directed Behavior; 3) Impulse Control Difficulties; 4) Lack of Emotional Awareness; 5) Limited Access to Emotion Regulation Strategies; and 6) Lack of Emotional Clarity. The score for each subscale is derived by calculating the average score for items of that subscale.

Participants with comorbid mood and anxiety disorders secondary to PTSD were included, as well as those with a history of substance dependence if abstinence had been maintained for more than three months. Regular psychotropic medication use was permitted only for antidepressant medication (5 participants used regular selective serotonin reuptake inhibitors throughout the duration of the study) as long as the

participant was stable on the same dosage, frequency, and type of medication for at least 3 months. Once entering the study, participants taking antidepressant medications were required to maintain the same medication dosage, frequency, and type throughout the duration of their participation. No other regular psychotropic medications were allowed. As-needed use of benzodiazepines was allowed up to three times per week and not within 48 hours of a scan, which was verbally verified by clinician or study team member. Other types of psychotropic medications such as mood stabilizers, antipsychotics, or anticonvulsants were not permitted, nor were regular use of thyroid medications or opiates. Participants were not allowed to have had any prior experience of prolonged exposure treatment, and no more than three sessions of any exposure-based psychotherapy. More extensive prior psychotherapy, i.e. more than 3 sessions, was allowable as long as it did not involve therapeutic exposure. This information was collected from the participant via self-report during the screening phase of the study.

General inclusion and exclusion criteria

Inclusion criteria for all participants encompassed the following: eligibility for scanning (i.e., no metal embedded in body, not currently pregnant, no history of severe claustrophobia), good English comprehension, currently meeting criteria for a PTSD diagnosis, and intellectual function adequate for comprehension of experimenter instructions. Exclusion criteria for all participants included: lifetime diagnosis of psychosis, bipolar disorder, intellectual disability, neurodevelopmental disorders, history of neurological conditions or organic mental disorder (e.g., stroke, seizures, tumor,

intracranial hemorrhage, multiple sclerosis), and substance dependence within the past three months.

Behavioral Paradigms

After completing baseline clinical assessment, those participants meeting eligibility criteria underwent functional magnetic resonance imaging (fMRI) on a separate day, which occurred prior to randomization. During scan acquisition, each participant completed three behavioral paradigms that probe components of emotional reactivity and regulation as well as one control task. Participants also underwent a high-resolution T1 structural scan for anatomical localization of BOLD signal. All behavioral paradigms were run on a Windows XP computer, projected onto a white screen at the base of the scanner bed, viewed by the participant using a mirror mounted above the head coil, and responded to via key press of a customized MRI-safe button box.

Emotional Reactivity Task: This previously-published paradigm (10) probes goal-irrelevant emotional reactivity via conscious and non-conscious (backwardly masked) presentation of fearful and neutral face stimuli. Faces were black and white photographs drawn from a standardized series developed by Ekman & Friesen (11), displayed in an elliptical shape that eliminated background and hair, and then artificially colorized in red, yellow, or blue and equalized for luminosity. Participants were instructed to identify, as quickly as possible, the color of the face via keypress of a button box. Importantly, identification or processing of the facial affect was only incidental and not the focus of the task. Faces displayed either fearful or neutral facial expressions and were presented

in a conscious and non-conscious format. Each trial lasted 2000 ms and began with presentation of a fixation cross to cue attention to the screen center (200ms) followed by a 400 ms latency period. Faces were then presented for 200ms, and participants were given 1200ms to respond with the color of the face presentation. For conscious presentation trials, one face (fearful or neutral) was presented for the entire 200ms. For the non-conscious masked fear condition, a fearful face was presented for 16.67 ms and then immediately backwards masked with a neutral face (in the same color tint and of the same gender, but with a different identity) for the remainder of the 200ms face presentation period (183.33ms). For the non-conscious masked neutral condition, the same backwards-masking procedure was utilized, but the initial quick prime was also a face with a neutral expression from a different individual than the masked face. Faces were presented in 16 blocks across one task run, with face color and gender randomized across blocks. Each block consisted of 10 face presentations of a particular emotion type and masked or unmasked. Four blocks of each emotion (fear or neutral) and masking combination (masked or unmasked) were presented in a counterbalanced format, resulting in 16 blocks total. Thus, there were 40 presentations of each face condition type, each lasting for 2000 ms. Stimuli were presented using Presentation software on a computer running Windows XP. Following completion of the color identification task while undergoing scanning, participants completed a forced-choice test (whether or not they saw a fearful face on each trial) using the same stimuli under the same conditions as the scanning procedure in order to assess adequacy of the masking procedure. This entire task lasted 9 minutes and 36 seconds (288 functional volumes acquired).

Emotional Conflict Task: This well-characterized paradigm (12, 13) assesses both emotional conflict and emotional conflict regulation, an implicit regulatory process in which the behavioral interference due to incongruent emotional stimuli is automatically suppressed from conflict trial to conflict trial. On each trial, participants were presented with an emotional face and instructed to identify the underlying facial emotion (fearful or happy) while ignoring an overlying emotion distractor (emotion word - “FEAR” or “HAPPY”) as quickly and accurately as possible. Trials varied such that emotional distractor words were either congruent or incongruent with the underlying facial expression. Each task consisted of 148 presentations of facial photographs drawn from a set by Ekman & Friesen (11), with 37 presentations of each stimulus type (congruent and incongruent fear and happy). Stimuli were presented for 1000 milliseconds (ms) in a fast event-related design with a varying inter-stimulus interval of 3000-5000 ms in a pseudo-randomized order counterbalanced for facial expression, gender, word, and response button. All participants of the study went through a practice version prior to entering the scanner to make sure proficiency (minimum 80% accuracy) was reached and the task instructions were understood. The entire task lasted 13 minutes and 14 seconds (397 functional volumes acquired).

Reappraisal Task: This emotion regulation task utilized here is described in a prior publication (14). In brief, the task consisted of presentation of 30 negative and 15 neutral photographs taken from the International Affective Picture System (IAPS) database. Each trial consisted of a 2 second cue presentation (“Look” or “Decrease”),

then a 7 second photo presentation, then a 4 second period to rate their level of emotional negativity at that moment using button box key press on a scale ranging from 1 (Not at all negative) to 5 (Very much negative). The scale was presented visually to participants during this period. There was then a 1 to 3 second rest period before the next cue presentation. Photographs were presented in a pseudorandom order such that no more than 2 of the same instruction (“Look” or “Decrease”) could be presented consecutively, and no more than 4 negative stimuli could be presented consecutively. Fifteen negative photographs were presented with a cue to “Look” and 15 were presented with a cue to “Decrease”, while all neutral photos were presented with a “Look” cue. Negative photographs depicted illness and/or injury (21 photos), acts of aggression (3 photos), members of hate groups (2 photos), transportation accidents (2 photos), and bodily waste (2 photos). Neutral photographs portrayed inanimate objects (10 photos) or neutral scenes (5 photos). Prior to undergoing the task, participants were instructed that, when cued to “Look”, they were to focus attention on the photo and allow their emotional reaction to occur naturally. When cued to “Decrease”, participants were instructed to attempt to reduce their emotional reaction to the photo by thinking of something that makes the photograph seem less negative to them (i.e. cognitive reappraisal). Participants were given practice examples of photographs and cognitive reappraisal strategies prior to entering the scanner, and they were also given the opportunity to practice reappraisal using their own spontaneously generated thought strategies on negative IAPS pictures (not utilized during scanning). The entire task lasted 11 minutes 28 seconds (344 functional volumes acquired). The contrasts of interest were looking at a negative picture vs. looking at a neutral picture (Look

Negative vs. Look Neutral) and using cognitive reappraisal to decrease negative emotion to a negative picture vs. looking at a negative picture (Decrease Negative vs. Look Negative).

Resting State: Participants completed an 8 minute eyes-open resting state scan (240 functional volumes acquired) in which they were told to lie still, try not to fall asleep, focus on a fixation cross, and allow their mind to wander. Subjects were debriefed afterwards to determine whether they fell asleep, and if so, the scan was repeated.

MRI Data Acquisition

Images were acquired on a 3-T GE Signa scanner using a custom-build head coil. During performance of each task, twenty-nine slices (4.0 mm thickness, 0.5 mm gap) were acquired in the axial direction across the whole brain using a T2*-weighted gradient echo spiral pulse sequence (TR = 2000 ms, TE = 30 ms, flip angle = 80°, 1 interleaf, field of view = 22 cm, 64x64 matrix). A high-resolution T1-weighted image (three-dimensional inversion recovery spoiled gradient-recalled acquisition in the coronal place with the following parameters: inversion time = 300 ms, TR = 8 ms, TE = 3.6 ms, flip angle = 15°, field of view = 22 cm, 124 slices, matrix = 256x192, number of excitations = 2, acquired resolution = 1.5 x 0.9 x 1.1 mm) was likewise obtained for each participant. During behavioral paradigms, measures of heart rate and respiration were collected and used to remove physiological noise from the time series (15).

Randomization

Following completion of baseline clinical assessments and fMRI scan, participants were individually randomized to one of two arms: 1) Immediate treatment with prolonged exposure therapy; or 2) Treatment waitlist. This occurred using random selection of a number from the string of digits 1 to 10, within an even selection indicating assignment to immediate treatment and an odd selection indicating assignment to waitlist. A total of sixty-six (N=66) individuals were randomized, with 36 being randomized to immediate treatment, and 30 to treatment waitlist. If randomized to immediate treatment, participants commenced treatment with a clinical psychologist trained to deliver prolonged exposure therapy. If randomized to waitlist, individuals were instructed they would have a 10-week waiting period after which they would undergo a second clinical assessment and fMRI scanning session. After completion of this second assessment, individuals on treatment waitlist were then assigned to a study therapist for completion of prolonged exposure therapy, which was provided for ethical reasons and not for neuroimaging analyses (since this would be outside of the randomized trial context).

Treatment Frequency and Length

Treatment sessions occurred on either a once or twice-weekly basis, for a total of either 9 or 12 90-minute sessions, according to manualized procedures (17). We chose to utilize a flexible treatment frequency format and allow for either once or twice-weekly sessions in order to reduce participant burden and minimally disrupt the participants' existing scheduled commitments. The variable duration of treatment (9 or 12 sessions)

was utilized in order to ensure that each participant received the maximal therapeutic benefit from prolonged exposure while also allowing for inter-individual differences in rate of therapeutic responses, which has been previously employed in similar treatment outcome designs (18). We note that allowing for this heterogeneity in treatment delivery could introduce other sources of variation that might impact response to the intervention. We examined this possibility post-hoc (see Supplemental Results), but it should be noted that these analyses are likely underpowered to detect such effects, if present.

At sessions 2, 4, 6, and 8 individuals were administered the PTSD-Checklist Civilian Version for DSM-IV (PCL-C)(6) as well as the Beck Depression Inventory-II (BDI-II)(5) to track response to treatment. The benchmark used to establish adequacy of treatment response at Session 9 and subsequent termination was a reduction in Session 8 PCL-C scores to less than 30% of the PCL-C total score at intake (i.e. 70% reduction from baseline)(18). If individuals met this benchmark, they were given the option to discontinue treatment after Session 9. If individuals did not meet this benchmark and/or wished to continue for an additional 3 sessions, treatment was terminated after Session 12. If treatment continued to 12 sessions, PCL and BDI measures were administered at Sessions 10 and 12.

Therapist Competency and Supervision in Prolonged Exposure

All psychologists received training in delivery of prolonged exposure and were deemed to meet competence in delivery of the treatment by one of the treatment developers, consultant to the study, and clinician supervisor Barbara Rothbaum, Ph.D.

Dr. Rothbaum provided weekly group supervision to study therapists and reviewed video recordings of treatment sessions to rate compliance with the treatment protocol and to provide supervision. Dr. Rothbaum watched the entirety of the first three treatment sessions for each therapist to ensure therapist familiarity and competence with all major components of the treatment (all delivered in the first three sessions), and she continued to review relevant portions of remaining sessions as directed by study therapists. All study therapists demonstrated good compliance with the therapy protocol and with no significant deviations, as demonstrated by good-to-excellent supervisor ratings of treatment session adherence.

Treatment Structure

Prolonged exposure therapy was delivered according to manualized procedures (17). All sessions were audio recorded on a digital voice recorder (entrusted to the participant to take home with them and for use in completing imaginal exposure homework assignments) as well as a digital video recorder (for the purposes of assessing treatment adherence, therapist competency, and clinical supervision). In brief, the structure and progression of treatment is as follows. Session 1 consisted of psychoeducation on posttraumatic stress disorder symptoms, the rationale for treatment, and treatment structure. It also involved additional assessment by the therapist of trauma history (including the index trauma, already established at intake), current symptoms, and current impairment. Breathing retraining was taught at the end of Session 1 and practiced collaboratively in session, which consisted of a normal inhalation and a controlled and slow exhalation with internal repetition of a calming word

or phrase (e.g., “Calm”) and a pause between exhalation and next inhalation, which was audiotaped for the participant. Session 2 consisted of homework review, self-report measures, a discussion of common reactions to trauma, a rationale for exposure as a treatment tool, construction of an exposure hierarchy for *in-vivo* exposure exercises, and selection of 2 to 3 hierarchy items for homework practice. Session 3 involved homework review, a brief rationale for imaginal exposure, and the first imaginal exposure in session for 45-60 minutes. This was followed by a processing portion in which the therapist and participant discussed the participant’s experience of the exposure, any insights received through that process, and areas to be further addressed in future exposures. Homework was then assigned (including completion of in-vivo exposures and imaginal exposures daily and practice of breathing retraining). Session 4 consisted of the same format as Session 3 but without the discussion of rationale for imaginal exposure.

Beginning in Session 5, the concept of trauma memory “hotspots” was discussed with participants, which were points in the memory during which the participant experienced the highest level of distress. The in-session imaginal exposure began to shift towards emphasizing hotspots in the memory in Session 5, at earliest, and sometimes Session 6 if agreed to be clinically appropriate by the participant and therapist. Sessions 6, 7, and 8 involved a similar format, with homework review, imaginal exposure to hot spots, processing, and homework assignment. For participants reaching the PCL clinical benchmark in Session 8, and agreeing to end in 9 sessions, Session 9 consisted of homework review, a brief imaginal exposure of the entire trauma memory conducted in-session (20-30 minutes), a brief processing, and a final review of

treatment progress and skills acquired. For participants not reaching the clinical benchmark and/or wishing to continue for an additional 3 sessions, Sessions 9-11 maintained the same format as Sessions 4-8. In this case, Session 12 served as the final session (which assumed the aforementioned format).

Post-Treatment Assessments

Approximately 4 weeks following the final treatment session, participants completed a post-treatment clinical assessment. A 4-week period was chosen to intercede between final session and post-treatment assessment in order to allow treatment changes to consolidate and symptom levels to equilibrate and to not overlap with the treatment period in assessing past-month PTSD symptoms. Moreover, brain changes from baseline noted at this time delay will be more representative of those changes conveying long-term therapeutic improvements. Participants were administered the CAPS and SCID again at post-treatment to assess change in PTSD symptoms and comorbid diagnoses. After completing the post-treatment clinical assessments, participants returned on another day to complete the post-treatment fMRI scan. Participants completed all of the same behavioral paradigms as in the baseline assessment, and another high-resolution T1 anatomical image was collected to assess potential structural brain changes arising from treatment.

Functional Image Preprocessing

Data were preprocessed using FSL tools (19). Affine transformation of functional to structural images using boundary-based registration based upon tissue segmentation

as implemented in FSL's FLIRT was added to non-linear normalization of each participant's T1 image to Montreal Neurological Institute (MNI) 152-person 1 mm^3 T1 template using FNIRT from FSL 5.0 (20). Functional images were subsequently aligned to the middle volume of the run. Global signal corresponding to segmented white matter and CSF was regressed out of motion-corrected functional images, which were isotropically smoothed with a 6 mm full-width half max (FWHM) to account for individual anatomical variability. For each time point (pre and post), participants with a root mean square absolute movement > 3mm across the mean of the squared maximum displacements in each of the 6 estimated translational and rotational motion parameters for each functional run were excluded from further analysis for quality control purposes. For pre-treatment scans, this amounted to 3 participants for the Emotional Reactivity task (2 in immediate treatment, 1 in waitlist), 3 participants for the Emotional Conflict Task (1 in immediate treatment, 2 in waitlist), 5 for the Reappraisal Task (3 in immediate treatment, 2 in waitlist), and 2 participants for resting state (0 in immediate treatment, 2 in waitlist). Thus, the final utilized sample size for the pre-treatment images were: N=63 for the Emotional Reactivity Task and the Emotional Conflict Task; N=61 for the Reappraisal Task; and N=64 for resting state. For post-treatment scans, this amounted to 2 participants for the Emotional Reactivity task (1 in immediate treatment, 1 in waitlist), 2 participants for the Emotional Conflict Task (1 in immediate treatment, 1 in waitlist), 5 participants for the Reappraisal Task (2 in immediate treatment, 3 in waitlist), and 2 participants for resting state (2 in immediate treatment, 0 in waitlist). Thus, the final utilized sample size (taken from the 50 study completers total, 24 in immediate treatment and 26 in waitlist) for the post-treatment images were: N=48 for the Emotional

Reactivity Task and the Emotional Conflict Task; N=45 for the Reappraisal Task; and N=48 for resting state.

Individual-Level Analysis of Functional Task Images

For each subject, time point, and task paradigm, regressors modeling trials of interest were convolved with the hemodynamic response function. First-level GLMs were conducted in SPM 8 (21) using relevant HRF-convolved regressors along with six parameters corresponding to nuisance regressors for within-session motion.

For the Emotional Reactivity task, regressors corresponded to the onset of facial stimuli for four conditions of interest: conscious fear, conscious neutral, non-conscious fear, and non-conscious neutral. The *a priori* contrasts of interest were the differences in activation for Conscious Fear vs. Conscious Neutral (F vs. N) and for Non-conscious Masked Fear vs. Non-conscious Masked Neutral (MF vs. MN), each allowing for the isolation of fear reactivity processes within a particular processing depth. As there was no non-facial comparator experimental condition included in this paradigm that could be used to examine activation magnitudes for each face type specifically, e.g., a scrambled face or shape processing condition, we note that this task's capacity for dissociating responses to fearful and neutral faces separately is limited. We therefore focused only on the assessment of within-subject contrast magnitudes (fearful minus neutral) for each processing depth (conscious or non-conscious), consistent with prior investigations utilizing this paradigm (10). Additionally, this contrast achieves the best experimental control, as it eliminates confounds including procedural aspects of the task and perception of facial features in general.

For the Emotional Conflict task, regressors corresponded to the onset of stimuli defined by face valence (Fear or Happy), congruency (Incongruent or Congruent), and prior trial type (Post-incongruent or Post-congruent) in order to model conflict regulation effects. This resulted in 8 different trial types in total, along with nuisance regressors for error trials and post-error trials (when applicable). The *a priori* contrasts of interest were Incongruent vs. Congruent trials (conflict), Post-incongruent Incongruent trials vs. Post-congruent Incongruent trials (iI vs. cI; an established measure of conflict regulation), and Congruent Fear vs. Congruent Happy trials, an additional probe of emotional reactivity to assess generalizability of effects from the Emotional Reactivity Task.

For the Reappraisal paradigm, regressors for the Look Neutral, Look Negative, and Reappraise Negative conditions were modeled from onset to offset of the picture stimulus to capture regulatory and reactivity processes. The *a priori* contrasts of interest here were Look Negative vs. Look Neutral (LookNeg vs. LookNeut), a measure of emotional reactivity to complex affective pictures, and Reappraise Negative vs. Look Negative (ReapNeg vs. LookNeg), a measure of cognitive reappraisal-related emotional regulatory activity which controls for picture valence and arousal-related processes.

Identifying Task-Related Activation

To identify task-related activation patterns across participants at baseline (i.e. unrelated to psychotherapy), individual subject contrast images for each task condition of interest were analyzed using threshold free cluster enhancement in FSL with a sign-flip permutation test (22). The distribution of effects was computed over 5,000 permutations per positive and negative side of the tail for each contrast, i.e. task effect.

The significance threshold was set at a family-wise error corrected $p < 0.05$ (two-tailed). Task effects were assessed in both a whole brain exploratory analysis as well as within an anatomically constrained region of interest mask specifying *a priori* brain structures relevant to PTSD and psychotherapy effects (Figure S1). This mask included the bilateral amygdala (derived from subcortical surface models implemented in FSL's subcortical segmentation program FIRST(23)), bilateral anterior insula (derived from the Automatic Anatomical Labeling (AAL) atlas (24), with the anterior portion defined as $y > 0$), anterior and mid-cingulate cortex ranging from the subgenual portion at its point adjoining the ventral striatum all the way up to dorsal anterior and mid-cingulate cortex (derived from the anterior cingulate, mid-cingulate, and olfactory cortex sites of the AAL atlas with $y > 0$, $-14 < x < 14$, and $-12 < z < 44$), and bilateral lateral and dorsolateral prefrontal cortex (defined as the bilateral inferior frontal, middle frontal, and superior frontal gyri from the AAL atlas constrained by $z > -4$, $16 < x < 60$ for right hemisphere, $-60 < x < -16$ for left hemisphere, and $y > -10$). Whole brain analyses were restricted to a probabilistic gray matter mask (> 40%) derived from an independent sample of healthy participants.

Individual-Level Analyses of Resting Brain Entropy

As a secondary analysis to support task-based findings, resting state images were analyzed using the Brain Entropy (BEN) Toolbox (25). This toolbox calculates a voxelwise measure of Sample Entropy (26), an extension of Approximate Entropy (27), both of which are approximations of Kolmogorov-Sinai complexity/entropy (28). Sample Entropy provides a stable measure of signal entropy that is stable across different

lengths of time course and across sessions (26, 29). Entropy is most properly a measure of system irregularity, which remains within a specified range in living systems but is constantly increasing over time in any closed system in accordance with the Second Law of Thermodynamics (30). In application to fMRI time series at rest, the human brain has been shown to display a consistent cortical distinction in regional entropy levels (25), with the outer neocortex displaying a uniformly lower level of entropy relative to subcortical gray and white matter. This demarcation is consistent with the highly organized structure of the human cerebral cortex (31), and the human brain at rest can be furthermore subdivided into hierarchically organized BEN networks that are consistent with structural and functional parcellations (25). Entropy can also be conceptualized as signal irregularity, signal complexity, or signal randomness (26). In the context of hemodynamic brain function, however, entropy could be considered a marker of accessibility to a variation of mental state changes over time, which manifest as a diversity in patterns of time course changes (32, 33). It has been previously utilized as a marker of brain state variability in electrophysiological investigations (34-37). Experimental evidence supports the contention that an optimal level of entropy, i.e. neither too high nor too low, is desirable, with certain diseases being characterized by restricted access to the variety of potential states available, i.e. reduced multiscale sample entropy (38), or abnormally-elevated entropy, i.e. highly disordered (32). Entropy reduction in the brain has been observed in Alzheimer's disease (35) as well as in normal aging, where lower entropy was associated with poorer cognitive function (39), though abnormally increased entropy was also observed in the context of multiple sclerosis where it was associated with greater disease severity (32).

The calculation of Sample Entropy can be conducted on any time series signal displaying properties of regularity/irregularity (26). The calculation begins by taking all consecutive time points in a time series and forming a series of embedded vectors with *m* consecutive time points extracted from the series (25). Using a pre-specified distance threshold, *r,* the algorithm calculates the number of vectors whose distances from each other are less than *r,* and this is also conducted for the vector length *m* + 1. By summating a vector number average weighted by the time series length and specified vector length for both *m* and *m* + 1, the value of Sample Entropy can be calculated as the negative natural log of the ratio of these two summations, with *m* in the denominator and *m* + 1 in the numerator (25). The values *m* and *r* are pre-defined in the algorithm by the user, with different *m* and *r* values providing different values for Sample Entropy, which is always a positive definite number with higher values indicating greater levels of entropy. The definition of Sample Entropy requires that *m* approaches ∞ as *r* approaches 0 (27). In practice, values of *m* typically utilized range between 2 and 4, and values of *r* typically vary from 0.3 to 0.6 (26). The values of *m*=3 and *r*=0.6 were empirically determined to provide the optimal brain entropy signal in a large resting-state fMRI sample (25). Thus, we utilized the same predefined values in the current analyses. It should be noted, however, that varying the value of *m* from 2 to 4 (in steps of 1) and *r* from 0.3 to 0.8 (in steps of 0.1) did not change the results.

In brief, resting state images were corrected for non-simultaneous slice acquisition, motion-corrected, intensity corrected for motion and physiological confounds due to heart rate, respiration, and white matter/CSF signal, temporally bandpass filtered ($0.009 < f < 0.08$), and smoothed with a 6mm full width half max

Gaussian kernel. The timeseries of each voxel across the whole-brain derived from motion-corrected and physiologically-denoised preprocessed resting state images was entered into a Sample Entropy calculation script compiled in C. Sample entropy was calculated both for the entire time series as well as downsampled data (odd and even number images averaged together) to provide an alternative temporal scale, which were then summed to provide a composite multi-scale measure of sample entropy (38) that is better differentiated from complex noise (such as pink noise or the 1/f process)(40). The resulting output was a brain map with a positive definite value at each voxel for the multi-scale Sample Entropy value of the timeseries, which was then spatially normalized to the MNI template. In order to control for potential nonspecific global effects and isolate regional changes, we normalized these Sample Entropy values within each individual by calculating the mean Sample Entropy level across the whole-brain, dividing each voxel by this value, and then subtracting 1 from that quotient (thus yielding a range of regional brain entropy values centered at 0, which denotes the mean level of Sample Entropy for that participant across the whole-brain). This method was utilized in the Brain Entropy Toolbox publication (25) to demonstrate whole-brain patterns of regional brain entropy, wherein the cerebral cortex displays a uniformly lower level of entropy, i.e. more regularity of timeseries signal, relative to white matter and subcortical structures. This whole-brain map of regional brain entropy values for each participant was then employed for group-level analyses to assess the impact of psychotherapy on regularity/complexity of BOLD signal at rest.

Assessing Treatment Effects

Clinical Measures

The effects of prolonged exposure on our primary clinical outcome (CAPS total score) as well as secondary outcomes of other symptom measures and quality of life were assessed in line with the intent-to-treat principle using a generalized linear mixed model with a robust estimator implemented in IBM SPSS 21 (41). We utilized a random intercept and fixed effects of time and treatment arm x time, with the latter fixed effect being the primary effect of interest (i.e., where trajectory of changes in the outcome measure were significantly different between the immediate treatment and waitlist arms). We furthermore required a significant parameter estimate for the time effect in the prolonged exposure group alone (i.e. where the change in trajectory for the outcome measure in the prolonged exposure group alone was significantly different from 0) in order to consider a treatment arm x time interaction as being derived from the prolonged exposure treatment. This was done to prevent interpretation of significant treatment arm x time interaction effects that were driven primarily by changes in the waitlist group, which would thus obscure the isolation of treatment-related effects.

Task Activation in Limbic Regions of Interest

To assess treatment-related brain changes in limbic regions of interest (anterior insula and amygdala), we utilized anatomical masks of the bilateral amygdalae (derived from subcortical surface models implemented in FSL's subcortical segmentation program FIRST(23)) and bilateral anterior insula (derived from the Automatic Anatomical Labeling (AAL) atlas (24), with the anterior portion defined as $y > 0$) to

extract an individual activation beta weight for each region within each subject for all tasks and contrasts of interest. These average activation values were then assessed in line with the intent-to-treat principle using a generalized linear mixed model with a robust estimator implemented in IBM SPSS 21 (41). As above, we utilized a random intercept and fixed effects of time and treatment arm x time, with the latter fixed effect being the primary effect of interest (i.e., where trajectory of changes in the outcome measure were significantly different between the immediate treatment and waitlist arms). We furthermore required a significant parameter estimate for the time effect in the prolonged exposure group alone (i.e. where the change in trajectory for the outcome measure in the prolonged exposure group alone was significantly different from 0) in order to consider a treatment arm x time interaction as being derived from the prolonged exposure treatment.

Voxelwise Analyses

To assess treatment-related brain changes on a voxel-wise level, we utilized AFNI's 3dLME program (42), which provides an interface to the R (43) statistical packages nlme (44) and lme4 (45). Consistent with the MacArthur approach (46) and in line with the intent-to-treat principle, we modeled the main effect of time and the treatment arm x time interaction, with the omnibus F statistic of the latter interaction being the primary outcome of interest. This effect indicates significantly different changes over time in the treatment group compared to the waitlist group. In addition, we also modeled the contrast estimates for pre vs. post treatment change within each arm separately in order to derive parameter estimates and significance of brain change from

pre- to post-treatment within each arm. To control for Type I error inflation, omnibus F-statistics for the treatment arm x time interaction effect were then subjected to voxel-level false discovery rate (FDR) correction ($q < 0.05$) within an independently derived whole brain gray matter mask and within a region of interest mask specifying *a priori* brain structures relevant to PTSD and psychotherapy effects (mask described above in *Identifying Task-Related Activation*). As an additional measure to verify treatment arm x time effects were driven by changes in the immediate treatment group, we only interpreted effects surviving the conjunction of the FDR-corrected omnibus F statistic map for the treatment arm x time interaction with the FDR-corrected t statistic map for the parameter estimate specifying a significant change from pre- to post-treatment within the immediate treatment group. Voxels surviving the $q < 0.05$ FDR correction conjunction were then clustered for the purposes of extraction, visualization, and verification using IBM SPSS 21.0. Generalized linear mixed models with a robust estimator were utilized to confirm significance of voxel-wise results.

Assessing Influence of the Left Lateral Frontopolar Cortex on the Ventromedial Prefrontal Cortex/Ventral Striatum in Healthy Participants

Scan Acquistion

To test the hypothesis that the frontopolar cortex exerts influence over the ventromedial prefrontal cortex/rostroventral striatum, we employed single-pulse transcranial magnetic stimulation (TMS) to the left frontopolar cortex in a separate sample of healthy participants undergoing concurrent fMRI ($n = 14$). This protocol was carried in in accordance with previously-published procedures (16) utilizing single

pulses of TMS interleaved with T2*-weighted volume acquisitions. Participants were recruited as part of an ongoing study examining TMS-induced functional connections in healthy participants. All participants were free of any current or lifetime history of psychopathology, verified by the Structured Clinical Interview for DSM-IV (3). In brief, a high-resolution T1-weighted SPGR inverted recovery 3D image was collected at a baseline task scanning session (300 ms after each inversion pulse, TE=8 ms, flip angle=15 deg, FOV=30cm, 128 axial slices, 256x192 matrix, two extractions, 1.5 x 0.9 x 1.1mm acquired resolution) and reconstructed as a 124x 256x 256 matrix with 1.5 x 0.9 x 0.9mm spatial resolution. This image was then calibrated with skin and scalp for individualized site targeting using Visor frameless stereotactic neuronavigation software (Magstim, Wales, UK) to define TMS stimulation sites for each participant prior to the TMS/fMRI scanning session. Participants wore a lycra swimcap to facilitate marking of stimulation sites. Motor threshold (MT) was defined as the lowest possible stimulation intensity at a site that induced a consistent visible response in the contralateral abductor pollicis brevis (thumb) muscle, a common within-subject metric for individualization of TMS intensity. Periods of single pulse TMS at 120% MT were interleaved with functional volumes acquired (concurrent fMRI). fMRI included oblique (axial to anatomy) slices of the full brain (31 slices, 4.0 mm thick, 1 mm gap) sampled via a T2* weighted gradient echo spiral pulse sequence (TR=2400, TE=30, flip angle=85 deg, 1 interleave, FOV=22 cm, 64x64 matrix) and using a 400 ms gap between volumes for TMS single pulse delivery. To counteract signal loss and blurring from local field inhomogeneities, high order shimming for spiral scans was done before acquisition. The left frontopolar cortex stimulation site was targeted using the Fp1 electrode from the 10/10 EEG coordinate

system, which was individual fitted to each participant prior to the concurrent TMS/fMRI scan. Primary motor cortex (M1) was defined using the MNI-152 anatomical atlas and then warped into subject native space using FSL's applywarp module (FMRIB, Oxford, UK). TMS target locations were identified within each subject's native space anatomical image after standardizing head position using nasion and bilateral tragi as fiducial markers within Visor. TMS was delivered via a MagVenture MR-compatible MRI-B91 figure-eight TMS coil held in place by a custom-built MRI coil holder, triggered by a MagVenture X100 stimulator located outside the room and connected to the coil via the penetration panel. The TMS sites were repositioned for each participant by sliding the participant out of the magnet bore, adjusting the coil position, and returning the participant into the bore. Single pulse TMS to the right hand knob of the primary motor cortex was used as an active comparison site. At each site, 68 TMS pulses were presented with a variable inter-trial interval jittered with delays of 2.4, 4.2, and 7.2 seconds delivered over 6 minutes and 41 seconds (167 volumes) in a fast event-related design. Pulses were delivered between collections of functional volumes to avoid corruption of BOLD signal.

Individual-Level Analysis

For each participant, regressors modeling trials of interest were convolved with the hemodynamic response function. For concurrent TMS-fMRI, the regressor of interested corresponded to "TMS on" periods for the left frontopolar cortex and the right hand knob of the primary motor cortex, and the contrast of left frontopolar cortex vs. right motor cortex stimulation served as the contrast of interest. First-level GLMs were

conducted in SPM 8.0 (21) using relevant HRF-convolved regressors along with six parameters corresponding to nuisance regressors for within-session motion.

Group-Level Analysis

To identify whether left frontopolar cortex stimulation can manipulate BOLD signal in the ventromedial prefrontal cortex/ventral striatum, we first extracted average BOLD signal change in the region defined by a mask of the cluster showing differential context-dependent connectivity change with the left frontopolar cortex during reappraisal in the treatment-randomized PTSD individuals. This was conducted within each participant and for each stimulation site. We then conducted a paired t-test of these average beta weights signifying BOLD signal change for each stimulation site (left frontopolar cortex and right motor cortex) to test for differential modulation of BOLD signal in this region as a function of stimulation site.

A voxelwise analysis was then conducted within a ventromedial prefrontal/ventral striatal region of interest defined by the mask of the treatment-related context-dependent connectivity change to verify the robustness of this effect to correction for multiple comparisons. Voxelwise analyses were conducted using threshold-free cluster enhancement (22) with a sign-flip permutation test on the within-subject contrasts of left frontopolar cortex stimulation vs. right motor cortex stimulation. The distribution of effects was computed over 5,000 permutations per positive and negative side of the tail for the contrast of left frontopolar vs. right motor cortex stimulation. The significance threshold was set at a family-wise error corrected $p < 0.05$ (two-tailed). Additional voxelwise analyses were also conducted within the extended *a priori* region of interest

mask utilized in the primary analyses as well as across the whole brain using the same technique.

Supplemental Results

Sample Characteristics

See CONSORT diagram (Figure S2) for complete details of participant recruitment, enrollment, and retention, and Table S2 for detailed information on sample characteristics and outcome data. The final randomized sample included 66 individuals, with 36 being randomized to immediate treatment and 30 randomized to waitlist. Of those randomized, 25 completed the post-treatment clinical assessment in the immediate treatment group, and 26 randomized to waitlist completed the post waitlist clinical assessment. Though there were a higher number of dropouts in the immediate treatment group, the difference in frequency of dropouts between groups was not statistically significant (two-tailed Fisher's exact test $p = 0.141$). Across groups, participants did not differ on age, education, PTSD symptom severity, or IQ. Comorbid major depression was equally represented in the immediate treatment and waitlist groups (50% in immediate treatment group, 56.67% in waitlist group; two-tailed Fisher's exact test $p = 0.628$), as was use of SSRI/SNRI medications (two-tailed Fisher's exact test $p = 1.00$, N=3 participants in treatment arm, N=2 participants in waitlist). In those individuals randomized to immediate treatment, 2 participants were taking an SSRI, and 1 participant was taking an SSRI and a benzodiazepine (with no usage 48 hrs. before a study appointment). In those individuals randomized to waitlist, 2 individuals were taking an SSRI, and there were no individuals taking a benzodiazepine (either alone or in combination with an SSRI). Thus, the groups were well matched on all relevant clinical and demographic variables. At the end of treatment/waitlist, none of the participants randomized to waitlist reached remission status from PTSD (operationalized as a CAPS

total score of less than or equal to 20). In those randomized to prolonged exposure treatment, however, 10 participants reached remission from PTSD while 15 participants continued to meet diagnostic criteria for the diagnosis.

Treatment Outcome

Consistent with expectation, individuals randomized to prolonged exposure demonstrated significantly greater reductions in CAPS total scores relative to those randomized to waitlist ($F = 20.05$, $p < 0.001$), and this effect was due to more robust symptom improvement in the treatment group (parameter estimate = -36.87, $t = -8.90$, $p < 0.001$) relative to waitlist (parameter estimate = -6.64, $t = -2.16$, $p = 0.036$). See Table S3 for post-treatment measure means. Additional significant time x treatment arm interactions were observed on depressive symptoms (BDI-II total score; $F = 4.272$, $p = 0.016$), wherein the treatment group (parameter estimate = -5.97, $t = -5.23$, $p < 0.001$) and the waitlist group (parameter estimate = -2.77, $t = -2.56$, $p = 0.014$) displayed reductions in BDI total scores from pre to post-assessments, but the reductions in the treatment arm were significantly larger. Time x treatment arm interactions were also observed on quality of life (WHO Quality of Life Scale BREF) in the domains of physical health ($F = 3.34$, $p = 0.039$) and psychological health ($F = 3.53$, $p = 0.033$), but not social relationships ($F = 1.07$, $p = 0.35$) nor environment ($F = 1.53$, $p = 0.22$). The interaction effect on physical health was due entirely to improvements in the treatment group (parameter estimate = 2.13, $t = 3.52$, $p = 0.001$) and not waitlist (parameter estimate = 0.27, $t = 0.56$, $p = 0.58$), and the interaction on psychological health was also driven by significant improvements in the treatment arm (parameter estimate = 3.15, $t =$

4.95, $p < 0.001$) with a trend for improvement in the waitlist arm (parameter estimate = 0.91, $t = 1.88$, $p = 0.066$).

Timeline of Participant Scans

After undergoing baseline clinical assessments and being enrolled into the study, participants completed their pre-treatment task-based fMRI scan. After the pre-treatment scan, individuals randomized to immediate treatment had their first session of prolonged exposure about one month later ($M = 29.9$ days, $SD = 10.9$ days). Within the treatment-randomized group, the average length of time from the pre-treatment fMRI session to the post-treatment fMRI session was about 13 weeks ($M = 90.1$ days, $SD = 22.67$ days), and the average length of time from the final treatment session to the post-treatment scan was about 4 weeks ($M = 28.67$ days, $SD = 8.50$ days). Within the waitlist-randomized group, the average length of time from the pre-waitlist fMRI session to the post-waitlist fMRI session was about 11 weeks ($M = 81.1$ days, $SD = 9.3$ days). Though the average length of time between pre and post scan sessions was slightly longer for treatment-randomized individuals, this difference was not significant ($t = 1.793$, $p = 0.083$).

Assessing Head Motion Differences Between Groups During Tasks

To verify that head motion during task completion was roughly equivalent between randomized groups, we utilized a multivariate GLM to examine motion parameters for group differences at pre and post scans, after excluding individuals with > 3mm root mean square absolute motion in any direction (as we did for group-level

analyses). Specifically, each GLM assessed for group differences across all motion parameters for each task at a particular time point. Thus, two GLMs were run—one for baseline scans and one for post-treatment/post-waitlist scans. For each task, we examined the following metrics: 1) root mean square of absolute displacement (total displacement in any direction from the image volume utilized for realignment); 2) root mean square of relative displacement (i.e. one volume to the next); 3) mean translation in x; 4) mean translation in y; 5) mean translation in z; 6) mean rotation around x; 7) mean rotation around 7; and 8) mean rotation around z.

At baseline, the multivariate effect of group was not significant (Pillai's Trace = 0.63, $F = 1.381$, $p = 0.201$). Additionally, the effect of group was nonsignificant across all of the univariate GLMs (all *p's* > 0.066). At post-treatment/post-waitlist, the multivariate effect of group was likewise not significant (Pillai's Trace = 0.822, $F = 1.013$, $p = 0.542$). Additionally, the effect of group was also non-significant across all of the univariate GLMS (all *p's* > 0.088).

Assessing the Impact of Treatment Frequency and Duration on Symptom Change

Of those individuals randomized to immediate treatment (N=36), 22 individuals underwent treatment once a week, and 14 individuals underwent treatment twice a week. In order to ascertain if these individuals systematically differed in important characteristics, we compared baseline demographic and symptom profiles between those individuals selecting to undergo treatment at different frequencies. These individuals did not differ in terms of demographics (age, education, gender), presence of comorbid major depression, or baseline PTSD symptoms (all *p's* > 0.15). We also

examined self-reported quality of life (WHO Quality of Life scale) across several domains, as different environmental characteristics (i.e. owning a car, having intact social relationships, being employed, etc.) could feasibly influence both quality of life and decision regarding treatment frequency. None of the domains of the WHO-Quality of Life Scale (physical, environmental, social, psychological, overall) significantly differed between individuals undergoing treatment at different frequencies (all *p's* < 0.12). We used linear mixed models in an intent-to-treat framework to examine the effect of treatment frequency on symptoms reductions. The frequency of treatment did not moderate the effect of treatment in the group randomized to prolonged exposure (Time x Treatment Frequency interaction $F = 0.53$, $p = 0.43$), and the effect of treatment on CAPS total scores was still highly significant when controlling for treatment frequency ($F = 88.38$, $p < 0.001$).

Next, we examined the effect of treatment duration (9 vs. 12 sessions) on the reported results. Of treatment completers (24 of 36 participants in those randomized to immediate treatment), 16 completed 12 sessions of prolonged exposure. Number of sessions completed did not relate to age, education, gender, or baseline PTSD symptoms (all *p's* > 0.25), nor did number of sessions completed relate to any domains of quality of life (all *p's* > 0.36). We next examined whether number of sessions completed influenced treatment outcomes. Using a linear mixed model in an intent-to-treat framework and examining treatment duration as a moderator of symptom reduction in the immediate treatment group, we observed that number of sessions of treatment completed did not moderate the effect of treatment on CAPS symptoms (Time x Treatment Duration $F = 0.20$, $p = 0.66$), and the effect of treatment was still significant

when controlling for duration of treatment (F = 6.49, p = 0.01). These results are consistent with the primary intent-to-treat analysis, which demonstrate that prolonged exposure was effective at reducing PTSD symptoms in an intent-to-treat framework.

Treatment Effects on Task Behavior

At baseline, there were no differences between groups on task behavior variables (all ***p's*** > 0.09). Following treatment, there was a time x treatment arm interaction on negativity ratings across all trial types of the Reappraisal paradigm (F = 9.07, p < 0.001) all of which were due to less negative emotion experienced at post assessment in the treatment-randomized individuals (t = -3.02, p = 0.003) but not waitlist (t = 0.75, p = 0.45). This reduction in negativity ratings did not differ as a function of trial type (F = 1.06, p = 0.37). There was no other significant time x treatment arm interaction observed on behavior in the Emotional Reactivity task or the Emotional Conflict paradigm (all ***p's*** < 0.11).

Baseline Task Activation

<u>Emotional Reactivity Task</u>

During conscious processing of fearful vs. neutral faces, the region of interest-constrained analysis revealed activation of the right middle frontal gyrus/inferior frontal gyrus, right anterior insula, and the middle cingulate cortex. No significant deactivations were detected for this contrast. In the whole brain exploratory analysis, additional activations were detected in the right precuneus/superior parietal lobule, brainstem, and

right mid-orbital gyrus. No significant deactivations were detected in the whole brain analysis.

During nonconscious processing of masked fearful vs. masked neutral faces, the region of interest-constrained analysis revealed activation of the left superior frontal gyrus, the right inferior frontal gyrus, and the right amygdala. No deactivations were detected. The whole brain analysis revealed additional activation of the brainstem, and deactivation was observed in the right hippocampus, right middle temporal gyrus, and right putamen.

Emotional Conflict Task

For the incongruent vs. congruent trial contrast, the region of interest-constrained analysis identified activation in the bilateral anterior insula, the left inferior frontal gyrus, and left superior frontal gyrus. No areas of deactivation were observed. In the whole brain exploratory analysis, large clusters of activation were detected in both hemispheres, extending from the temporal pole through the insula, putamen, inferior frontal gyrus, middle frontal gyrus, superior frontal gyrus, and precentral gyrus, with the cluster in the left hemisphere continuing to extend into the medial frontal gyrus, and middle cingulate cortex. Additional areas of activation observed included the left inferior parietal lobule/supramarginal gyrus/angular gyrus, bilateral middle cingulate cortex, left middle temporal gyrus, midbrain, right precentral gyrus, and right inferior parietal lobule. No areas of deactivation were detected in the whole brain analysis.

In the congruent fear vs. congruent happy contrast, the region of interest-constrained analysis detected activation in the left inferior frontal gyrus. No clusters of

deactivation were observed. In the whole brain analysis, additional activation was observed in the right middle temporal gyrus, and deactivation was observed in the left hippocampus.

In the conflict regulation contrast (post-incongruent incongruent vs. post-congruent incongruent trials), the region of interest-constrained analysis revealed activation of the pregenual anterior cingulate cortex and deactivation of the bilateral inferior frontal gyrus/middle frontal gyrus/superior frontal gyrus and middle cingulate cortex. The exploratory whole brain analysis revealed no additional activations, but it identified very large clusters of deactivation spanning multiple regions of the dorsolateral and dorsomedial prefrontal cortex as well as lateral and medial parietal cortex.

Reappraisal Task

The region of interest-constrained analysis of the Look Negative vs. Look Neutral contrast revealed activation of the right middle frontal gyrus, left anterior insula, left dorsal anterior cingulate, and the left amygdala. There were no areas of deactivation observed. The whole brain exploratory analysis yielded additional activation in the bilateral cuneus, left middle occipital gyrus, and right inferior occipital gyrus/fusiform gyrus, and deactivation was observed in the left lingual gyrus and left postcentral gyrus.

The region of interest-constrained analysis of the Reappraise Negative vs. Look Negative contrast yielded activation of the right inferior and middle frontal gyri (P. Opercularis and P. Triangularis), the left middle and superior frontal gyri, and the right anterior insula. There were no areas of deactivation observed. The whole brain

exploratory analysis yielded additional extended activation in large posterior portions of both hemispheres, including visual cortex, inferior and lateral temporal cortex, and precuneus, as well as the bilateral supplementary motor area and motor cortex.

Assessing Selectivity of Left Lateral Frontopolar Activation Change to Reappraisal

As the detection of a significant treatment arm x time interaction on brain activation in one task or contrast but not another could reflect a more task-general effect that fails to reach significance in some comparisons, we investigated the selectivity of left lateral frontopolar activation change during reappraisal by extracting average left lateral frontopolar activation within each participant during each task contrast (conscious fear vs. neutral and masked fear vs. masked neutral from the emotional reactivity task; incongruent vs. congruent, post-incongruent incongruent vs. post-congruent incongruent; and congruent fear vs. congruent happy from the emotional conflict task; and look negative vs. look neutral and reappraise negative vs. look negative from the reappraisal task) at first and second scans. We utilized a mask of the activation change effect detected in the left frontopolar cortex during reappraisal to derive an average activation value for each participant at each time point and for each task contrast of interest. We then subjected these average left frontopolar activation values to a generalized linear mixed model with a robust estimator to examine the time x treatment arm x task contrast interaction effect. If left lateral frontopolar activation change is selective to the reappraisal contrast, we would expect to see a significant time x treatment arm x task contrast interaction effect. The analysis demonstrated a significant time x treatment arm x task contrast interaction ($F = 4.135$, $p < 0.001$). Follow-up mixed

models within each task contrast demonstrated a significant time x treatment arm interaction effect for the reappraise negative vs. look negative contrast of the Reappraisal paradigm only ($F = 17.526$, $p < 0.001$), with the same effect for lateral frontopolar activation change not reaching significance for any other task contrast (all *p's* > 0.11).

Assessing the Impact of Treatment Frequency and Duration on Brain Changes

First, we examined whether treatment frequency interacted with any of the brain activation, connectivity, or resting entropy changes. To do this, we examined the interaction of treatment frequency with the effect of time on frontopolar activation change, change in frontopolar connectivity with the ventromedial prefrontal cortex/ventral striatum during reappraisal, and change in frontopolar resting entropy (using extracted average beta weights or sample entropy values from clusters identified in the voxel-wise analyses) in an intent-to-treat framework. By necessity, this analysis was conducted only in those individuals randomized to immediate treatment, as individuals randomized to waitlist would not have any assigned value for treatment frequency. These analyses showed that treatment frequency did not interact with the effect of Time in the treatment group to influence: a) frontopolar activation change during reappraisal (all $p = 0.25$); b) change in frontopolar connectivity with ventromedial prefrontal cortex/ventral striatum during reappraisal ($p = 0.46$); nor c) change in frontopolar resting entropy ($p = 0.154$). Moreover, the effect of Time within the immediate treatment group continued to remain significant in all models (*p's* < 0.004).

Next, we examined whether treatment duration moderated brain activation, connectivity, and resting entropy changes using linear mixed models in an intent-to-treat framework. We modeled this effect as the interaction of Time with treatment duration on frontopolar activation, connectivity with the ventromedial prefrontal cortex/ventral striatum during reappraisal, and frontopolar resting entropy (analogous to the analysis for treatment frequency reported above). We observed that treatment duration did not interact with the effect of Time in the treatment group to influence: a) frontopolar activation change ($p = 0.928$); b) change in frontopolar connectivity with the ventromedial prefrontal cortex/ventral striatum during reappraisal ($p = 0.596$); nor c) change in frontopolar resting entropy ($p = 0.40$). Additionally, the effect of Time continued to remain significant in these models ($p's < 0.04$).

Assessing the Impact of Psychiatric Medication on Brain Changes

Finally, to determine whether medication usage might impact the brain change results, we excluded the 5 subjects on psychoactive medications and re-ran the brain activation, connectivity, and resting entropy change analyses using extracted individual average beta weights for activation, connectivity, and resting entropy from clusters identified in the primary voxelwise analyses. The findings were unchanged, with change in frontopolar activation during reappraisal still remaining highly significant ($p < 0.001$) as well as change in frontopolar connectivity with the ventromedial prefrontal cortex/ventral striatum ($p = 0.002$) and frontopolar change in resting entropy ($p < 0.001$). We also ran an additional set of analyses in which we included the entire sample and specified a variable corresponding to the use of medication (SSRI or benzodiazepine).

We then examined this variable in interaction with differential change over time due to treatment (Time x Group x Med Use) controlling for all lower-order interactions and main effects. The use of medication did not significantly interact with frontopolar activation change, change in frontopolar connectivity with the ventromedial prefrontal cortex/ventral striatum, nor change in frontopolar resting entropy (all *p's* > 0.09). Though these post-hoc analyses are likely underpowered to detect significant interactions of treatment duration, frequency, or medication usage with brain changes, they suggest that no large-magnitude interaction effects were clearly present.

Relationships Between Task Behavior Change and Symptom Change

As negativity ratings during the Reappraisal paradigm were the only task behavioral metrics that showed significant differential treatment-related changes, we examined the relationship between symptom change (CAPS total scores) and change in negativity ratings during this paradigm to establish if these task behavior changes were related to symptom improvement. Using change scores for CAPS total scores and negativity ratings during the reappraisal paradigm (pre minus post) and controlling for baseline symptoms and reappraisal distress ratings in a generalized linear model with a robust estimator, we observed that greater reduction in PTSD symptoms in the treatment arm was associated with greater reduction in negativity ratings for the Look Negative condition (Wald χ^2=10.51, p = 0.001), the Decrease Negative condition (Wald χ^2=25.93, p < 0.001), and the Look Neutral condition (Wald χ^2=5.60, p = 0.018). These relationships were not significant in the waitlist arm (all *p's* > 0.14).

Examining Differential Brain Changes by PTSD Remission Status: Exploratory Analyses

We undertook additional analyses to determine: a) whether there were additional brain changes not detected in the primary analyses that differed as a function of PTSD remission status at the end of treatment; and b) whether the changes detected in the primary analyses differed as a function of PTSD remission status. Remission was chosen as a metric to examine potential differential brain changes as a function of treatment efficacy since it is clinically meaningful and also split the treatment sample fairly evenly (10 remitted, 15 non-remitted in the immediate treatment group; no remitters in waitlist). Individuals were classified as diagnostic remitters or non-remitters according to a widely utilized clinical research criterion of post-treatment CAPS total score less than or equal to 20 (47).

First, we conducted additional analyses on extracted average activation values in limbic regions of interest to look for differential changes across time using a three group split: waitlist (none of whom reached remission), remitters following immediate treatment, and non-remitters following immediate treatment. We conducted these analyses the same way as the primary analyses reported in the initial manuscript, i.e. using average within-subject activation values within four *a priori* regions of interest (left amygdala, right amygdala, left anterior insula, right anterior insula) and running a generalized linear mixed model in SPSS (41) to test for differential activation change as a function of the aforementioned three group-split based on remission status and randomization arm. One model was run for each region of interest within each task contrast of interest. Convergent with the results of the primary limbic analyses, these remission analyses revealed no significant time x remission group effects across any

region of interest for any contrast examined (all *p's* > 0.084, uncorrected for multiple comparisons).

Next, we ran voxelwise analyses on all of the task contrasts examined to look for differential changes across time using the same three group split: waitlist (none of whom reached remission), remitters following immediate treatment, and non-remitters following immediate treatment. We conducted these analyses the same way as the primary analyses reported in the manuscript, i.e. using voxelwise linear mixed models and voxel level FDR control for multiple comparisons within our regions of interest and across the whole brain. This was also conducted for frontopolar connectivity during reappraisal as well as resting entropy. We observed no additional significant effects that survived correction for multiple comparisons. In other words, there was no differential brain change detected as a function of remission status from pre- to post-treatment across any of the metrics examined in the primary analyses.

We then examined the brain changes detected in primary analyses for differential changes as a function of remission status. Using extracted average beta weights for frontopolar cortical activation, the Remission Group x Time effect continued to remain significant ($p < 0.001$), and the parameters specifying change in activation continued to remain significant in both the remitters ($p = 0.037$) and the non-remitters ($p = 0.048$). Moreover, within the immediate treatment group, we examined whether remission status moderated the change in brain activation as a function of time. The interaction of Time x Remission status was not significant ($p = 0.732$).

The same was true for frontopolar cortical connectivity change with the ventromedial prefrontal cortex. The Remission Group x Time effect continued to remain

significant (p = 0.02), and the parameters specifying change in connectivity in both the remitters (p = 0.078) and the non-remitters (p = 0.087) still approached significance and were similar in direction and magnitude (remitters: 0.21; non-remitters: 0.19). Additionally, within the treatment group remission status at the end of treatment did not moderate the change in frontopolar connectivity with the ventromedial prefrontal cortex (p = 0.893).

Finally, we examined resting entropy for differential changes as a function of treatment status in the frontopolar cortex. The Remission Group x Time effect continued to remain significant (p < 0.001), and the parameters specifying change in resting entropy in both the remitters (p = 0.036) and non-remitters (p = 0.083) continued to remain at or trend towards significance, with similar direction and magnitude (remitters: 0.043, non-remitters: 0.038). Within those individuals randomized to immediate treatment, remission status at the end of the study did not moderate the change in frontopolar resting entropy (p = 0.977).

Summary and Limitations

It should be noted these analyses are no longer in line with the intent-to-treat principle (since the grouping variable is now defined based upon completion status as well as original randomization), and they are likely underpowered to detect significant differences in brain changes between remitters and non-remitters following prolonged exposure. However, they suggest that the changes detected in the primary analyses are treatment-general rather than contingent upon a particular level of treatment response.

Testing Intrinsic Resting State Functional Connectivity Between the Left Lateral Frontopolar Cortex and the Ventromedial Prefrontal Cortex/Ventral Striatum for Treatment-Related Changes

In addition to investigating resting state brain entropy, we also tested whether the left lateral frontopolar cortex and ventromedial prefrontal cortex/ventral striatum displayed changes in intrinsic functional connectivity at rest in addition to during the reappraisal task. Using the same pre-processed images that were employed for resting entropy analyses (corrected for non-simultaneous slice acquisition, motion-corrected, intensity corrected for motion and physiological confounds due to heart rate, respiration, and white matter/CSF signal, temporally bandpass filtered ($0.009 < f < 0.08$), and smoothed with a 6mm full width half max Gaussian kernel), we extracted the average time course of signal changes from the regions identified in voxelwise analyses as showing treatment-related change during the reappraisal task and examined their r-to-z transformed correlation coefficients at pre and post scans. Using a generalized linear mixed model with a robust estimator, we observed no significant treatment arm x time effect ($p = 0.52$) on connectivity between the left frontopolar cortex and the ventromedial prefrontal cortex/ventral striatum.

Left Frontopolar TMS-Induced Modulation of Ventromedial Prefrontal/Ventral Striatal BOLD Signal in Healthy Individuals: Voxelwise Analyses

In addition to comparing average signal change in healthy individuals in the ventromedial prefrontal cortex/ventral striatal area defined by the differential context-

dependent connectivity change in treatment-randomized PTSD patients, we conducted additional voxelwise analyses to verify the robustness of this effect. Within a region of interest mask defined by the context-dependent connectivity change effect, we observed significantly greater deactivation in the subgenual anterior cingulate portion of the ventromedial prefrontal cortex (Brodmann Area 25) extending into the nucleus accumbens and caudate head (Table S8). This effect was due to deactivation from baseline in the left frontopolar stimulation condition (t = -5.32, p < 0.001) with no change from baseline in the right motor cortex stimulation condition (t = 0.76, p = 0.46). This effect did not survive comparison for multiple corrections when utilizing the full *a priori* region of interest mask used in the primary voxelwise analyses. A whole brain exploratory analysis identified an additional region of significantly lower BOLD signal for left frontopolar stimulation vs. right motor cortex stimulation in the left lingual gyrus/calcarine gyrus (Table S8). This effect was driven both by deactivation in the left frontopolar stimulation condition (t = -4.01, p = 0.002) and activation in the right motor cortex stimulation condition (t = 2.65, p = 0.021). No effects for increased BOLD signal for left frontopolar stimulation vs. right motor cortex stimulation were observed.

Supplemental References

1. Fonzo GA, Goodkind MS, Oathes DJ, Zaiko YV, Harvey M, Peng KK, Weiss ME, Thompson AL, Zack SE, Lindley SE, Arnow BA, Jo B, Gross JJ, Rothbaum BO, Etkin A. PTSD psychotherapy outcome predicted by brain activation during emotional reactivity and regulation. Am J Psychiatry (doi: 10.1176/appi.ajp.2017.16091072).
2. Blake DD, Weathers FW, Nagy LM, Kaloupek DG, Gusman FD, Charney DS, Keane TM. The development of a Clinician-Administered PTSD Scale. Journal of traumatic stress. 1995;8:75-90.
3. First MB, Spitzer RL, Gibbon M, Williams JBW: Structured Clinical Interview for DSM-IV-TR Axis I Disorders, Research Version, Patient Edition (SCID-I/P). New York, Biometrics Research, New York State Psychiatric Institute; 2002.
4. Wechsler D: Wechsler Abbreviated Scale of Intelligence. New York, NY, The Psychological Corporation: Harcourt Brace & Company; 1999.
5. Beck AT, , Steer RA, , Brown GK, . Manual for Beck Depression Inventory-II. 1996.
6. Weathers F, Litz B, Herman D, Huska J, Keane T: The PTSD Checklist (PCL): Reliability, Validity, and Diagnostic Utility. in Annual Convention for the International Society for Traumatic Stresss Studies. San Antonio, TX1993.
7. Skevington SM, , Lotfy M, , O'Connell KA, . The World Health Organization's WHOQOL-BREF quality of life assessment: psychometric properties and results of the international field trial. A report from the WHOQOL group. 2004;13:299-310.
8. Gross JJ, John OP. Individual differences in two emotion regulation processes: Implications for affect, relationships, and well-being. Journal of Personality and Social Psychology. 2003;85:348-362.
9. Gratz KL, Roemer L. Multidimensional Assessment of Emotion Regulation and Dysregulation: Development, Factor Structure, and Initial Validation of the Difficulties in Emotion Regulation Scale. Journal of Psychopathology and Behavioral Assessment. 2004;26:41-54.
10. Etkin A, Klemenhagen KC, Dudman JT, Rogan MT, Hen R, Kandel ER, Hirsch J. Individual differences in trait anxiety predict the response of the basolateral amygdala to unconsciously processed fearful faces. Neuron. 2004;44:1043-1055.

11. Ekman P FW. Pictures of facial affect. . Consulting Psychologists Palo Alto, CA. 1976.
12. Etkin A, Egner T, Peraza DM, Kandel ER, Hirsch J. Resolving emotional conflict: a role for the rostral anterior cingulate cortex in modulating activity in the amygdala. Neuron. 2006;51:871-882.
13. Etkin A, Prater KE, Hoeft F, Menon V, Schatzberg AF. Failure of anterior cingulate activation and connectivity with the amygdala during implicit regulation of emotional processing in generalized anxiety disorder. Am J Psychiatry. 2010;167:545-554.
14. Minkel JD, McNealy K, Gianaros PJ, Drabant EM, Gross JJ, Manuck SB, Hariri AR. Sleep quality and neural circuit function supporting emotion regulation. Biology of mood & anxiety disorders. 2012;2:22.
15. Glover GH, Li TQ, Ress D. Image-based method for retrospective correction of physiological motion effects in fMRI: RETROICOR. Magnetic resonance in medicine. 2000;44:162-167.
16. Chen AC, Oathes DJ, Chang C, Bradley T, Zhou ZW, Williams LM, Glover GH, Deisseroth K, Etkin A. Causal interactions between fronto-parietal central executive and default-mode networks in humans. Proc Natl Acad Sci U S A. 2013;110:19944-19949.
17. Foa EB, Hembree EA, Rothbaum BO: Prolonged Exposure Therapy for PTSD. Oxford, Oxford University Press; 2007.
18. Foa EB, Hembree EA, Cahill SP, Rauch SA, Riggs DS, Feeny NC, Yadin E. Randomized trial of prolonged exposure for posttraumatic stress disorder with and without cognitive restructuring: outcome at academic and community clinics. Journal of consulting and clinical psychology. 2005;73:953-964.
19. Jenkinson M, Beckmann CF, Behrens TE, Woolrich MW, Smith SM. FSL. Neuroimage. 2012;62:782-790.
20. Andersson JLR JM, Smith S Non-linear registration, a.k.a. spatial normalisation. FMRIB Technical Report. 2010.
21. Penny W, Friston K, Ashburner J, Kiebel S, Nichols T. Statistical Parametric Mapping: The Analysis of Functional Brain Images. Statistical Parametric Mapping: The Analysis of Functional Brain Images. 2007:1-680.

22. Smith SM, Nichols TE. Threshold-free cluster enhancement: addressing problems of smoothing, threshold dependence and localisation in cluster inference. Neuroimage. 2009;44:83-98.
23. Patenaude B, Smith SM, Kennedy DN, Jenkinson M. A Bayesian model of shape and appearance for subcortical brain segmentation. Neuroimage. 2011;56:907-922.
24. Tzourio-Mazoyer N, Landeau B, Papathanassiou D, Crivello F, Etard O, Delcroix N, Mazoyer B, Joliot M. Automated anatomical labeling of activations in SPM using a macroscopic anatomical parcellation of the MNI MRI single-subject brain. Neuroimage. 2002;15:273-289.
25. Wang Z, Li Y, Childress AR, Detre JA. Brain entropy mapping using fMRI. PloS one. 2014;9:e89948.
26. Richman JS, Moorman JR. Physiological time-series analysis using approximate entropy and sample entropy. American journal of physiology Heart and circulatory physiology. 2000;278:H2039-2049.
27. Pincus SM. Approximate entropy as a measure of system complexity. Proc Natl Acad Sci U S A. 1991;88:2297-2301.
28. Kolmogorov AN. On Tables of Random Numbers. Sankhyā: The Indian Journal of Statistics, Series A (1961-2002). 1963;25:369-376.
29. Lake DE, Richman JS, Griffin MP, Moorman JR. Sample entropy analysis of neonatal heart rate variability. American journal of physiology Regulatory, integrative and comparative physiology. 2002;283:R789-797.
30. Borgnakke C, Sonntag RE: Fundamentals of Thermodynamics2014.
31. Gomez-Robles A, Hopkins WD, Schapiro SJ, Sherwood CC. Relaxed genetic control of cortical organization in human brains compared with chimpanzees. Proc Natl Acad Sci U S A. 2015;112:14799-14804.
32. Zhou F, Zhuang Y, Gong H, Zhan J, Grossman M, Wang Z. Resting State Brain Entropy Alterations in Relapsing Remitting Multiple Sclerosis. PloS one. 2016;11:e0146080.
33. Strange BA, Duggins A, Penny W, Dolan RJ, Friston KJ. Information theory, novelty and hippocampal responses: unpredicted or unpredictable? Neural networks : the official journal of the International Neural Network Society. 2005;18:225-230.

34. Rezek IA, Roberts SJ. Stochastic complexity measures for physiological signal analysis. IEEE transactions on bio-medical engineering. 1998;45:1186-1191.
35. Poza J, Hornero R, Escudero J, Fernandez A, Sanchez CI. Regional analysis of spontaneous MEG rhythms in patients with Alzheimer's disease using spectral entropies. Annals of biomedical engineering. 2008;36:141-152.
36. Bruna R, Poza J, Gomez C, Garcia M, Fernandez A, Hornero R. Analysis of spontaneous MEG activity in mild cognitive impairment and Alzheimer's disease using spectral entropies and statistical complexity measures. Journal of neural engineering. 2012;9:036007.
37. Fernandez A, Hornero R, Gomez C, Turrero A, Gil-Gregorio P, Matias-Santos J, Ortiz T. Complexity analysis of spontaneous brain activity in Alzheimer disease and mild cognitive impairment: an MEG study. Alzheimer disease and associated disorders. 2010;24:182-189.
38. Costa M, Goldberger AL, Peng CK. Multiscale entropy analysis of biological signals. Physical review E, Statistical, nonlinear, and soft matter physics. 2005;71:021906.
39. Yang AC, Huang CC, Yeh HL, Liu ME, Hong CJ, Tu PC, Chen JF, Huang NE, Peng CK, Lin CP, Tsai SJ. Complexity of spontaneous BOLD activity in default mode network is correlated with cognitive function in normal male elderly: a multiscale entropy analysis. Neurobiol Aging. 2013;34:428-438.
40. Wang Z: Personal communication via e-mail. Edited by Fonzo GA2016.
41. IBM SPSS Statistics for Macintosh, Version 21.0. Armonk, NY, IBM Corp; 2012.
42. Chen G, Saad ZS, Britton JC, Pine DS, Cox RW. Linear mixed-effects modeling approach to FMRI group analysis. Neuroimage. 2013;73:176-190.
43. Team RC: R: A language and environment for statistical computing. 3.2.3 ed. Vienna, Austria, R Foundation for Statistical Computing; 2015.
44. Jose P, Douglas B, Saikat D, Sarkar D, Team. RC: nlme : Linear and Nonlinear Mixed Effects Models. 2015.
45. Bates D, Machler M, Bolker BM, Walker SC. Fitting Linear Mixed-Effects Models using lme4. Journal of Statistical Software. 2015;67:1-48.

46. Kraemer HC, Wilson GT, Fairburn CG, Agras WS. Mediators and moderators of treatment effects in randomized clinical trials. Archives of general psychiatry. 2002;59:877-883.
47. Weathers FW, Ruscio AM, Keane TM. Psychometric properties of nine scoring rules for the clinician-administered Posttraumatic Stress Disorder Scale. Psychological Assessment. 1999;11:124-133.
48. Levin P, Lazrove S, van der Kolk B. What psychological testing and neuroimaging tell us about the treatment of Posttraumatic Stress Disorder by Eye Movement Desensitization and Reprocessing. J Anxiety Disord. 1999;13:159-172.
49. Farrow TF, Hunter MD, Wilkinson ID, Gouneea C, Fawbert D, Smith R, Lee KH, Mason S, Spence SA, Woodruff PW. Quantifiable change in functional brain response to empathic and forgivability judgments with resolution of posttraumatic stress disorder. Psychiatry research. 2005;140:45-53.
50. Lansing K, Amen DG, Hanks C, Rudy L. High-resolution brain SPECT imaging and eye movement desensitization and reprocessing in police officers with PTSD. The Journal of neuropsychiatry and clinical neurosciences. 2005;17:526-532.
51. Felmingham K, Kemp A, Williams L, Das P, Hughes G, Peduto A, Bryant R. Changes in anterior cingulate and amygdala after cognitive behavior therapy of posttraumatic stress disorder. Psychol Sci. 2007;18:127-129.
52. Peres JF, Newberg AB, Mercante JP, Simao M, Albuquerque VE, Peres MJ, Nasello AG. Cerebral blood flow changes during retrieval of traumatic memories before and after psychotherapy: a SPECT study. Psychological medicine. 2007;37:1481-1491.
53. Lindauer RJ, Booij J, Habraken JB, Meijel EP, Uylings HB, Olff M, Carlier IV, Heeten GJ, Eck-Smit BL, Gersons BP. Effects of psychotherapy on regional cerebral blood flow during trauma imagery in patients with post-traumatic stress disorder: a randomized clinical trial. Psychological medicine. 2008;38:543-554.
54. Rabe S, Zoellner T, Beauducel A, Maercker A, Karl A. Changes in brain electrical activity after cognitive behavioral therapy for posttraumatic stress disorder in patients injured in motor vehicle accidents. Psychosom Med. 2008;70:13-19.
55. Roy MJ, Francis J, Friedlander J, Banks-Williams L, Lande RG, Taylor P, Blair J, McLellan J, Law W, Tarpley V, Patt I, Yu H, Mallinger A, Difede J, Rizzo A, Rothbaum

B. Improvement in cerebral function with treatment of posttraumatic stress disorder. Ann N Y Acad Sci. 2010;1208:142-149.
56. Adenauer H, Catani C, Gola H, Keil J, Ruf M, Schauer M, Neuner F. Narrative exposure therapy for PTSD increases top-down processing of aversive stimuli--evidence from a randomized controlled treatment trial. BMC neuroscience. 2011;12:127.
57. Dickie EW, Brunet A, Akerib V, Armony JL. Neural correlates of recovery from post-traumatic stress disorder: a longitudinal fMRI investigation of memory encoding. Neuropsychologia. 2011;49:1771-1778.
58. Peres JF, Foerster B, Santana LG, Fereira MD, Nasello AG, Savoia M, Moreira-Almeida A, Lederman H. Police officers under attack: resilience implications of an fMRI study. Journal of psychiatric research. 2011;45:727-734.
59. Thomaes K, Dorrepaal E, Draijer N, de Ruiter MB, Elzinga BM, van Balkom AJ, Smit JH, Veltman DJ. Treatment effects on insular and anterior cingulate cortex activation during classic and emotional Stroop interference in child abuse-related complex post-traumatic stress disorder. Psychological medicine. 2012;42:2337-2349.
60. Aupperle RL, Allard CB, Simmons AN, Flagan T, Thorp SR, Norman SB, Paulus MP, Stein MB. Neural responses during emotional processing before and after cognitive trauma therapy for battered women. Psychiatry research. 2013;214:48-55.
61. Simmons AN, Norman SB, Spadoni AD, Strigo IA. Neurosubstrates of remission following prolonged exposure therapy in veterans with posttraumatic stress disorder. Psychotherapy and psychosomatics. 2013;82:382-389.
62. van Rooij SJ, Geuze E, Kennis M, Rademaker AR, Vink M. Neural correlates of inhibition and contextual cue processing related to treatment response in PTSD. Neuropsychopharmacology : official publication of the American College of Neuropsychopharmacology. 2015;40:667-675.
63. King AP, Block SR, Sripada RK, Rauch S, Giardino N, Favorite T, Angstadt M, Kessler D, Welsh R, Liberzon I. ALTERED DEFAULT MODE NETWORK (DMN) RESTING STATE FUNCTIONAL CONNECTIVITY FOLLOWING A MINDFULNESS-BASED EXPOSURE THERAPY FOR POSTTRAUMATIC STRESS DISORDER (PTSD)

IN COMBAT VETERANS OF AFGHANISTAN AND IRAQ. Depression and anxiety. 2016;33:289-299.

FIGURE S1. Anatomical Regions of Interest Utilized for Voxelwise Analyses

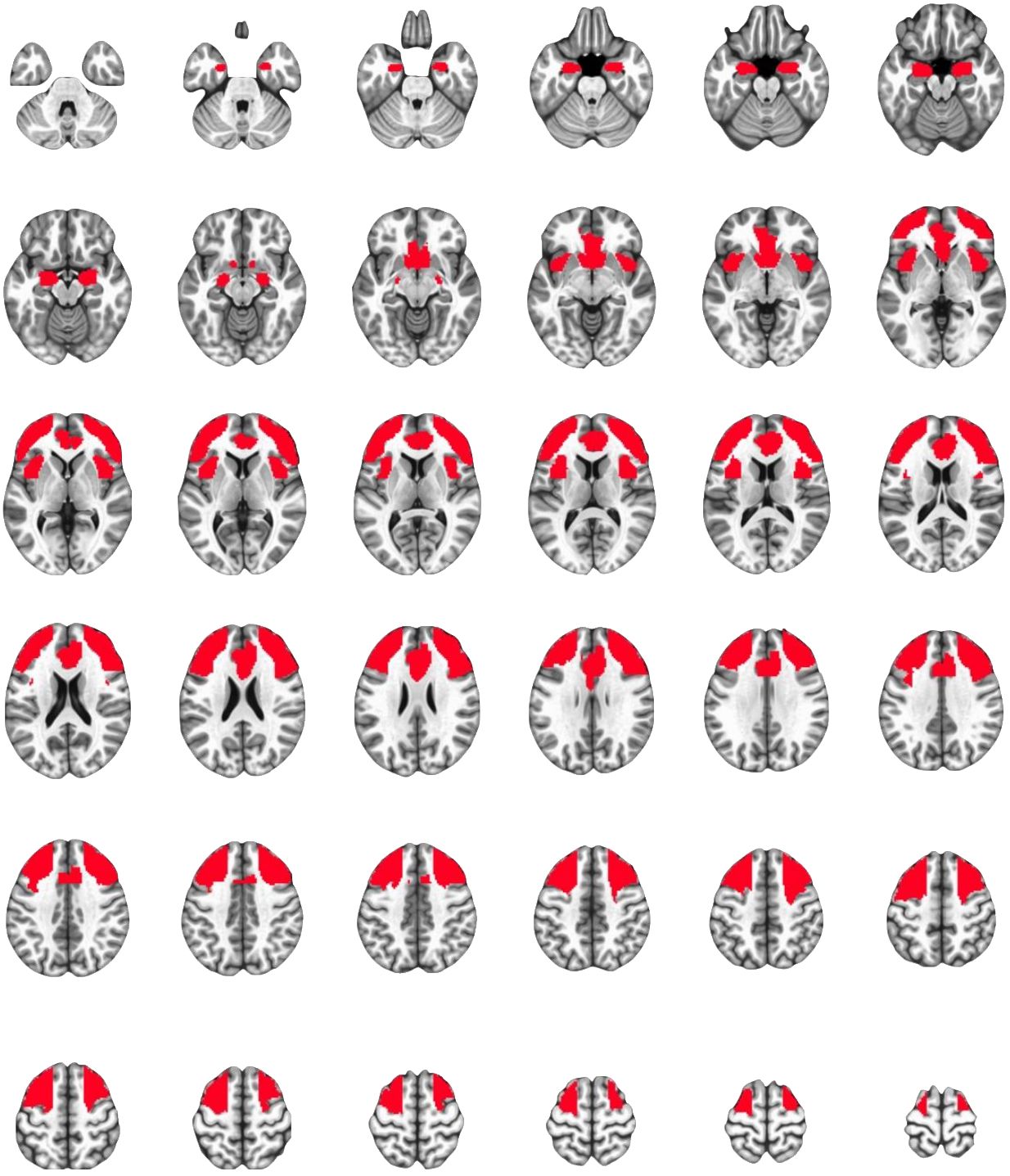

Figure depicts the anatomical regions of interest utilized for voxelwise analyses overlaid upon the Montreal Neurological Institute average brain with 3mm spacing of slices in the axial plane. Regions of interest included the amygdala, anterior insula, dorsal and ventral anterior cingulate cortex, anterior mid-cingulate cortex, and lateral prefrontal cortex ranging from anterior (frontopolar) to posterior (dorsolateral).

FIGURE S2. CONSORT Diagram

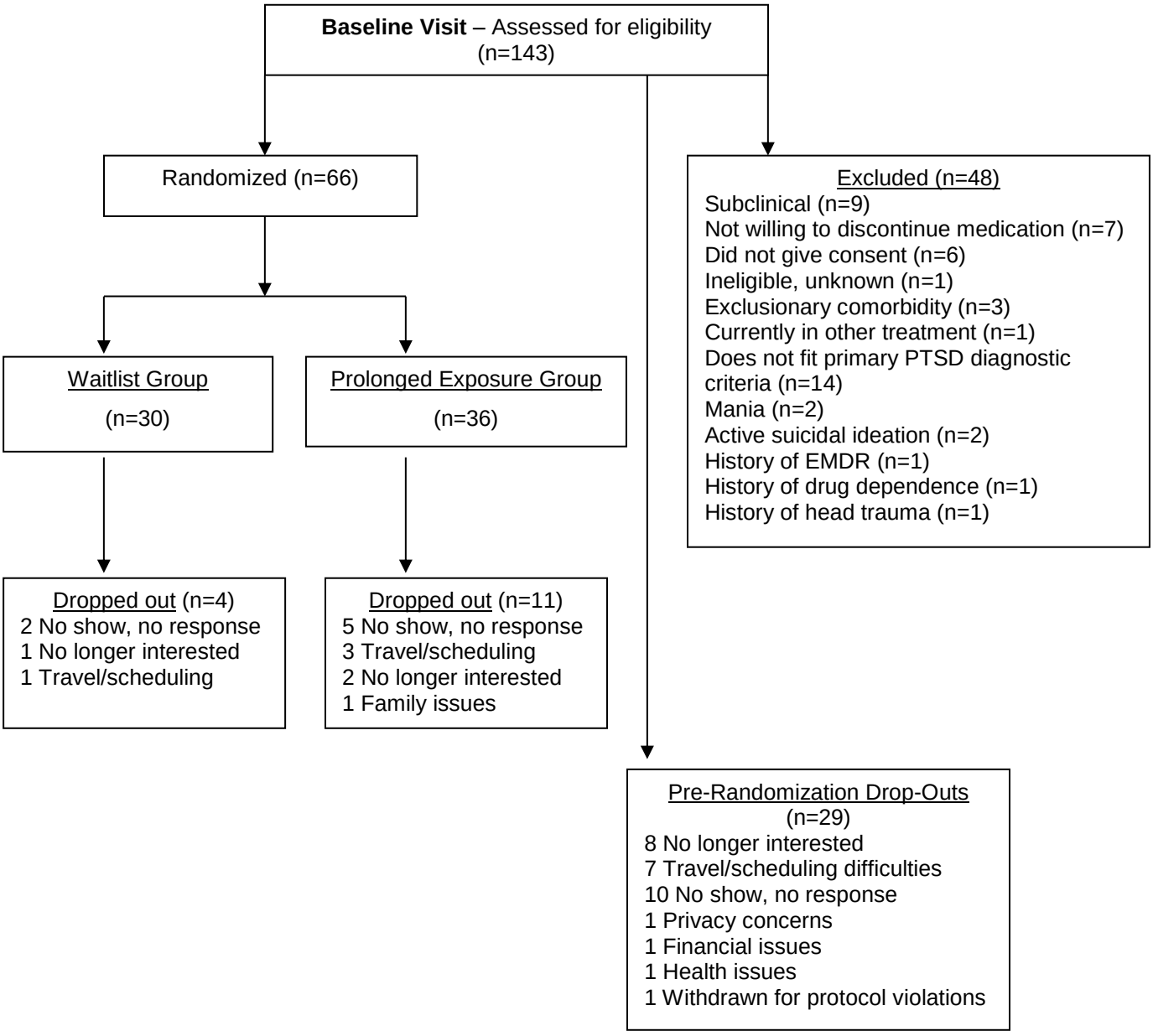

TABLE S1. Previously Published PTSD Psychotherapy Functional Imaging Studies of Brain Changes

(Ref) Author, Year	PMID	Sample	Design	Task(s)	Imaging Method
(48) Levin et al., 1999	10225506	PTSD (N=1)	Case study, pre/post, EMDR	Recall of trauma memory	SPECT
(49) Farrow et al., 2005	16213690	PTSD (N=13)	Pre/post, CBT w/ forgiveness component	Forgivability judgments of other's actions	fMRI
(50) Lansing et al., 2005	16387993	PTSD (N=6)	Pre/post, EMDR	Connors Continuous Performance Task	SPECT
(51) Felmingham et al., 2007	17425531	PTSD (N=8)	Pre/post, CBT	Fear/neutral faces	fMRI
(52) Peres et al., 2007	17288648	Sub-threshold PTSD: Tx (N=16) and WL (N=11)	RCT, ETCR	Script-driven symptom provocation	SPECT
(53) Lindauer et al., 2008	17803835	PTSD: Tx (N=10) and WL (N=10), TEHC (N=15)	RCT, BEP	Trauma script-driven imagery	SPECT
(54) Rabe et al., 2008	17991819	PTSD or sub-syndromal PTSD: Tx (N=17), WL (N=18)	RCT, CBT	Emotional vs. neutral picture viewing	EEG
(55) Roy et al., 2010	20955336	PTSD (N=8)	Pre/post, VRET or PE	Affective Stroop	fMRI
(56) Adenauer et al., 2011	22182346	PTSD: Tx (N=16) and WL (N=18)	RCT, NET	Aversive vs. neutral picture viewing	MEG

TABLE S1 (cont). Previously Published PTSD Psychotherapy Functional Imaging Studies of Brain Changes

(57) Dickie et al., 2011	21382385	PTSD (N=32)	Pre/post, TAU	Memory for faces and scenes	fMRI
(58) Peres et al., 2011	21159352	Partial PTSD: Tx (N=12) and WL (N=12), TEHC (N=12)	RCT, ETCR	Retrieval of traumatic memory	fMRI
(59) Thomaes et al., 2012	22436595	PTSD: PECBSGT + TAU (N=9) and TAU (N=7)	RCT, PECBSGT	Classic Stroop and Emotional Stroop	fMRI
(60) Aupperle et al., 2013	23916537	PTSD (N=14)	Pre/post, CTT-BW	Anticipation and viewing of positive and negative images	fMRI
(61) Simmons et al., 2013	24061484	PTSD: Remitted (N=9) and Non-remitted (N=15)	Pre/post, PE	Anticipation and viewing of positive and negative images	fMRI
(62) van Rooij et al., 2015	25154707	PTSD: Responder (N=22) and Non-responder (N=17), TEHC (N=22)	Pre/post, TAU	Stop signal task	fMRI
(63) King et al., 2016	27038410	PTSD: MBET (N=14) or PCGT (N=9)	RCT, MBET vs. PCGT	Resting state	fMRI

BEP=brief eclectic psychotherapy; CBT=cognitive-behavioral therapy; CTT-BW=cognitive trauma therapy for battered women; EEG=electroencephalography; EMDR=eye movement desensitization and reprocessing; ETCR=exposure therapy with cognitive restructuring; fMRI=functional magnetic resonance imaging; MBET=mindfulness-based exposure therapy; MEG=magnetoencephalography; NET=narrative exposure therapy; PCGT=present-centered group therapy; PE=prolonged exposure; PMID=PubMed ID; PECBSGT=psycho-educational and cognitive-behavioral stabilizing group treatment; PTSD=posttraumatic stress disorder; RCT=randomized clinical trial; SPECT=single photon emission computed tomography; TAU=treatment as usual; TEHC=trauma-exposed healthy control; Tx=treatment; VRET=virtual reality exposure therapy; WL=waitlist.

TABLE S2. Demographic and Pretreatment Clinical Characteristics of Participants With PTSD Assigned to Either Immediate Prolonged Exposure Treatment or a Waiting List Condition

Measure	Immediate Treatment Group (N=36)		Waiting List Group (N=30)	
	Mean	SD	Mean	SD
Age (years)	34.42	10.23	39.03	10.35
Education (years)	14.72	2.17	15.17	2.78
Full-scale IQ (Wechsler Abbreviated Scale of Intelligence)	109.03	9.09	112.81	11.57
	N	%	N	%
Female	23	64	20	66
Diagnosis of major depression at intake[a]	18	50	17	57
Completed the study	25	69	26	87
Clinician-Administered PTSD Scale for DSM-IV				
Index trauma				
Natural disaster	3	8	1	3
Physical assault	9	25	7	23
Assault with a weapon	3	8	2	7
Sexual assault	12	33	9	30
Combat exposure	4	11	4	13
Injury, illness, suffering	5	14	7	23
Developmental stage at time of index trauma				
Adult	20	56	14	47
Teen	8	22	11	37
Child	8	22	5	17
How exposed to index trauma				
Experienced	27	75	17	57
Witnessed	9	25	13	43
Index trauma repeated	11	31	10	33
Multiple criterion A events	12	33	10	33
	Mean	SD	Mean	SD
Total score	66.33	15.17	71.37	14.99
Reexperiencing subscale	17.53	6.40	18.73	6.02

TABLE S2 (cont). Demographic and Pretreatment Clinical Characteristics of Participants With PTSD Assigned to Either Immediate Prolonged Exposure Treatment or a Waiting List Condition

Avoidance/numbing subscale	26.94	7.86	28.77	8.89
Hyperarousal subscale	21.86	6.28	23.87	4.91
Beck Depression Inventory–II	23.69	8.68	23.17	8.60
PTSD Checklist for DSM-IV–Civilian Version				
Total	56.16	10.61	57.36	12.04
Reexperiencing subscale	16.47	3.83	16.29	3.98
Avoidance/numbing subscale	22.78	5.05	23.04	6.02
Hyperarousal subscale	16.91	4.22	18.04	4.19
WHO Quality of Life BREF Scale				
Physical health subscale	12.46	2.99	12.43	3.11
Psychological health subscale	10.04	2.29	10.83	2.34
Social relationships subscale	9.71	4.06	9.29	3.51
Environment subscale	12.30	3.48	12.79	3.37

[a] Three patients in the immediate treatment group and two in the waiting list group were taking selective serotonin and/or norepinephrine reuptake inhibitors at baseline.

TABLE S3. Posttreatment Symptom and Quality-of-Life Measures in Participants With PTSD Assigned to Either Immediate Prolonged Exposure Treatment or a Waiting List Condition

	Immediate Treatment Group (N=36)		Waiting List Group (N=30)				
Measure	**Mean**	**SD**	**Mean**	**SD**	**F or χ^2**	**p**	**Cohen's d**
Clinician-Administered PTSD Scale for DSM-IV							
Total	29.60	21.26	64.23	21.77	32.99	<0.001	1.61
Reexperiencing subscale	6.20	6.49	16.92	7.97	27.62	<0.001	1.48
Avoidance/numbing subscale	10.60	9.50	24.50	11.30	22.51	<0.001	1.33
Hyperarousal subscale	12.80	8.75	22.81	7.00	20.43	<0.001	1.26
Beck Depression Inventory–II	9.69	7.77	17.87	9.27	11.23	0.002	0.96
PTSD Checklist for DSM-IV–Civilian Version							
Total	26.13	7.80	49.00	13.35	45.55	<0.001	2.09
Reexperiencing subscale	7.41	2.63	14.38	5.14	31.76	<0.001	1.71
Avoidance/numbing subscale	10.36	3.36	19.24	6.32	33.46	<0.001	1.75
Hyperarousal subscale	8.41	3.11	15.38	4.15	39.05	<0.001	1.90
WHO Quality of Life BREF Scale							
Physical health subscale	14.63	3.29	12.65	3.19	4.09	0.049	0.61
Psychological health subscale	13.19	2.59	11.94	2.52	2.63	0.11	0.49
Social relationships subscale	11.83	3.20	10.73	3.20	1.29	0.26	0.34
Environment subscale	14.59	2.42	13.57	2.99	1.55	0.22	0.38

TABLE S4. Task Dependent Activations/Deactivations At Baseline

Task	Contrast	Mask	Hem.	MNI Atlas Region(s)	# Voxels	X	Y	Z
Emo Reac	F-N	ROI	R	Middle Frontal Gyrus/Inferior Frontal Gyrus (P. Triangularis)	738	44	21	31
Emo Reac	F-N	ROI	R	Insula Lobe	231	38	13	-4
Emo Reac	F-N	ROI	R	Middle Frontal Gyrus	110	27	3	51
Emo Reac	F-N	ROI	L/R	Middle Cingulate Cortex	84	4	16	38
Emo Reac	F-N	WB	R	Middle Frontal Gyrus/Inferior Frontal Gyrus (P. Triangularis)	590	44	19	32
Emo Reac	F-N	WB	R	Superior Parietal Lobule/Precuneus	568	19	-65	59
Emo Reac	F-N	WB	R	Insula Lobe/Temporal Pole	350	45	16	-13
Emo Reac	F-N	WB	L/R	Brainstem	118	0	-33	-52
Emo Reac	F-N	WB	R	Middle Frontal Gyrus/Inferior Frontal Gyrus (P. Triangularis)	32	51	47	5
Emo Reac	F-N	WB	R	Mid-Orbital Gyrus	23	12	61	-4
Emo Reac	MF-MN	ROI	L	Superior Frontal Gyrus	17	-26	10	68
Emo Reac	MF-MN	ROI	R	Middle Frontal Gyrus	6	36	24	22
Emo Reac	MF-MN	ROI	R	Amygdala	3	24	-8	-13
Emo Reac	MF-MN	WB	L/R	Brainstem	39	6	-21	-45
Emo Reac	MF-MN	WB	R	Hippocampus (-)	53	24	-40	6
Emo Reac	MF-MN	WB	R	Middle Temporal Gyrus (-)	27	64	0	-22
Emo Reac	MF-MN	WB	R	Putamen	13	20	10	-2
Emo Con	Inc-Con	ROI	L	Insula Lobe	360	-36	17	7
Emo Con	Inc-Con	ROI	R	Insula Lobe	308	39	18	6
Emo Con	Inc-Con	ROI	L	Superior Frontal Gyrus	167	-27	-5	63
Emo Con	Inc-Con	ROI	L	Inferior Frontal Gyrus (P. Triangularis)	135	-40	20	24
Emo Con	Inc-Con	WB	L	Putamen/Insula Lobe/Temporal Pole/Inferior Frontal Gyrus (P. Triangularis/P. Opercularis)/Precentral Gyrus/Middle Frontal Gyrus/Superior Frontal Gyrus/SMA/Middle Cingulate Cortex	6243	-24	6	39
Emo Con	Inc-Con	WB	R	Insula Lobe/Temporal Pole/Inferior Frontal Gyrus (P. Triangularis/P. Opercularis)/Precentral Gyrus/Middle Frontal Gyrus	2095	42	15	12
Emo Con	Inc-Con	WB	L	Middle Occipital Gyrus/Supramarginal Gyrus/Angular Gyus/Inferior Parietal Lobule/Superior Parietal Lobule	1813	-34	-56	41
Emo Con	Inc-Con	WB	L/R	Middle Cingulate Cortex	493	0	-25	30

TABLE S4 (cont). Task Dependent Activations/Deactivations At Baseline

Task	Contrast	Mask	Hem.	MNI Atlas Region(s)	# Voxels	X	Y	Z
Emo Con	Inc-Con	WB	L	Middle Temporal Gyrus	395	-52	-53	11
Emo Con	Inc-Con	WB	L/R	Midbrain	206	-1	-28	-12
Emo Con	Inc-Con	WB	R	Precentral Gyrus	66	31	-15	55
Emo Con	Inc-Con	WB	R	Inferior Parietal Lobule	27	34	-47	39
Emo Con	FvH	ROI	L	Inferior Frontal Gyrus (P. Triangularis)	29	-40	20	24
Emo Con	FvH	WB	R	Middle Temporal Gyrus	17	54	-34	4
Emo Con	FvH	WB	L	Hippocampus (-)	12	-24	-18	-22
Emo Con	iI-cI	ROI	L/R	Anterior Cingulate	10	0	36	0
Emo Con	iI-cI	ROI	R	Superior Frontal Gyrus/Middle Frontal Gyrus/Inferior Frontal Gyrus (P. Triangularis) (-)	3232	40	33	23
Emo Con	iI-cI	ROI	L	Superior Frontal Gyrus/Middle Frontal Gyrus/Inferior Frontal Gyrus (P. Triangularis) (-)	1109	-37	38	18
Emo Con	iI-cI	ROI	L/R	Middle Cingulate Cortex (-)	410	5	17	37
Emo Con	iI-cI	ROI	L	Middle Frontal Gyrus (-)	167	-26	-4	58
Emo Con	iI-cI	ROI	R	Insula Lobe (-)	119	33	21	3
Emo Con	iI-cI	WB	L	Temporal Pole/Inferior Frontal Gyrus (P. Triangularis)/Superior Frontal Gyrus/Middle Frontal Gyrus/Rolandic Operculum/Precentral Gyrus/Anterior Cingulate/Supramarginal Gyrus/Superior Occipital Gyrus/Inferior Parietal Lobule/Superior Parietal Lobule/Postcentral Gyrus/Middle Cingulate Cortex/SMA (-)	9778	-25	-5	43
Emo Con	iI-cI	WB	R	Putamen/Insula Lobe/Pallidum/Inferior Frontal Gyrus (P. Triangularis)/Superior Frontal Gyrus/Middle Frontal Gyrus/Precentral Gyrus (-)	5035	39	20	24
Emo Con	iI-cI	WB	R	Middle Temporal Gyrus/Superior Temporal Gyrus/Middle Occipital Gyrus/Supramarginal Gyrus/Angular Gyrus/Superior Parietal Lobule/Inferior Parietal Lobule/Superior Occipital Gyrus/Postcentral Gyrus/Precuneus (-)	4070	32	-54	46
Emo Con	iI-cI	WB	L	Supramarginal Gyrus (-)	40	-57	-47	28
Reap	LNeg-Neut	ROI	R	Middle Frontal Gyrus	383	36	10	26
Reap	LNeg-Neut	ROI	L	Insula Lobe	321	-44	16	12
Reap	LNeg-Neut	ROI	L	Anterior Cingulate	314	-2	-4	30
Reap	LNeg-Neut	ROI	L	Amygdala	3	-24	2	-20
Reap	LNeg-Neut	WB	L/R	Cuneus	996	-4	-74	20
Reap	LNeg-Neut	WB	L	Middle Occipital Gyrus	285	-30	-90	-4
Reap	LNeg-Neut	WB	R	Inferior Occipital Gyrus/Fusiform Gyrus	154	36	-66	-10
Reap	LNeg-Neut	WB	L	Lingual Gyrus (-)	190	-10	-86	-2

TABLE S4 (cont). Task Dependent Activations/Deactivations At Baseline

Task	Contrast	Mask	Hem.	MNI Atlas Region(s)	# Voxels	X	Y	Z
Reap	LNeg-Neut	WB	L	Postcentral Gyrus (-)	127	-46	-18	54
Reap	Reap-LNeg	ROI	R	Middle Frontal Gyrus/Inferior Frontal Gyrus (P. Triangularis/P. Opercularis)	2579	33	14	43
Reap	Reap-LNeg	ROI	L	Middle Frontal Gyrus/Superior Frontal Gyrus	540	-27	-1	55
Reap	Reap-LNeg	ROI	R	Insula Lobe	216	35	13	0
Reap	Reap-LNeg	WB	L/R	Cerebellum/Cerebellar Vermis/Fusiform Gyrus/Inferior Temporal Gyrus/Lingual Gyrus/Inferior Occipital Gyrus/Middle Occipital Gyrus/Middle Temporal Gyrus/Calcarine Gyrus/Superior Occipital Gyrus/Superior Temporal Gyrus/Cuneus/Supramarginal Gyrus/Precuneus/Postcentral Gyrus/Inferior Parietal Lobule/Angular Gyrus/Superior Parietal Lobule	26132	9	-69	11
Reap	Reap-LNeg	WB	L	Superior Temporal Gyrus/Rolandic Operculum/Postcentral Gyrus/Supramarginal Gyrus/Precentral Gyrus/Inferior Parietal Lobule	2049	-44	-18	41
Reap	Reap-LNeg	WB	R	Inferior Frontal Gyrus (P. Opercularis/P. Triangularis)/Middle Frontal Gyrus/Precentral Gyrus	1965	41	7	37
Reap	Reap-LNeg	WB	L/R	Superior Medial Gyrus/SMA	361	3	21	49
Reap	Reap-LNeg	WB	L	Superior Parietal Lobule	125	-23	-59	49
Reap	Reap-LNeg	WB	R	Precentral Gyrus	30	25	-13	67

X, Y, and Z values are cluster center of mass coordinates in MNI stereotactic space; A negative (-) sign following the MNI Atlas regions indicates that cluster was a deactivation; Task column specifies the functional task from which the cluster was identified, while the contrast column specifies the contrast of task conditions; Emo Con = emotional conflict task; Emo Reac = emotional reactivity task; F-N = conscious (unmasked) fear vs. neutral faces; FvH = congruent fear vs. congruent happy trials; iI-cI = conflict regulation (post-incongruent incongruent trials vs. post-congruent incongruent trials); Inc-Con = incongruent vs. congruent trials; L = left; LNeg-Neut = look negative vs. look neutral trials; MF-MN = nonconscious (masked) fear vs. neutral faces; MNI = Montreal Neurological Institute; R = right; Reap = reappraisal task; Reap-LNeg = reappraise negative vs. look negative trials; ROI = region of interest; WB = whole brain.

TABLE S5. Amygdala and Anterior Insula Region of Interest Analyses of Differential Activation Change By Treatment Arm

Task	Contrast	Hem.	Region	Time Effect	Treatment Arm x Time Effect	PreTx Value		PostTx Value	
						PE	WL	PE	WL
Emo Reac	F-N	L	Ant Ins	F = 1.045, p = 0.311	F = 0.788, p = 0.457	0.002 (0.139)	0.043 (0.168)	0.032 (0.170)	0.065 (0.099)
Emo Reac	F-N	R	Ant Ins	F = 0.039, p = 0.844	F = 0.618, p = 0.541	0.019 (0.152)	0.062 (0.158)	0.027 (0.186)	0.037 (0.109)
Emo Reac	F-N	R	Amyg	F = 0.038, p = 0.846	F = 0.580, p = 0.562	0.013 (0.256)	0.021 (0.215)	0.053 (0.214)	-0.003 (0.152)
Emo Reac	F-N	L	Amyg	F = 0.591, p = 0.444	F = 1.511, p = 0.225	0.038 (0.227)	-0.017 (0.189)	0.070 (0.218)	0.015 (0.156)
Emo Reac	MF-MN	L	Ant Ins	F = 1.321, p = 0.256	F = 0.158, p = 0.692	0.029 (0.160)	-0.102 (0.186)	0.001 (0.150)	0.012 (0.132)
Emo Reac	MF-MN	R	Ant Ins	F = 0.867, p = 0.356	F = 0.718, p = 0.399	0.026 (0.158)	-0.054 (0.128)	-0.001 (0.163)	0.036 (0.148)
Emo Reac	MF-MN	R	Amyg	F = 0.661, p = 0.418	F = 2.445, p = 0.121	0.005 (0.256)	0.006 (0.211)	-0.083 (0.213)	0.015 (0.163)
Emo Reac	MF-MN	L	Amyg	F = 0.137, p = 0.712	F = 1.097, p = 0.297	-0.008 (0.204)	0.006 (0.221)	-0.048 (0.202)	0.014 (0.200)
Emo Con	Inc-Con	L	Ant Ins	F = 5.399, p = 0.024*	F = 0.040, p = 0.842	0.282 (0.567)	0.286 (0.481)	0.055 (0.694)	0.020 (0.507)
Emo Con	Inc-Con	R	Ant Ins	F = 4.718, p = 0.034*	F = 0.000, p = 0.985	0.170 (0.529)	0.385 (0.623)	0.011 (0.687)	0.010 (0.678)
Emo Con	Inc-Con	R	Amyg	F = 3.151, p = 0.082	F = 0.032, p = 0.858	-0.001 (0.688)	0.003 (0.442)	-0.237 (0.672)	-0.236 (0.951)
Emo Con	Inc-Con	L	Amyg	F = 1.765, p = 0.190	F = 0.900, p = 0.345	-0.047 (0.670)	-0.049 (0.495)	-0.300 (0.774)	-0.103 (0.613)
Emo Con	FvH	L	Ant Ins	F = 0.190, p = 0.664	F = 0.000, p = 0.988	-0.065 (0.963)	0.568 (1.044)	0.295 (0.887)	0.299 (0.765)
Emo Con	FvH	R	Ant Ins	F = 0.329, p = 0.568	F = 0.110, p = 0.741	0.096 (0.960)	0.534 (0.929)	0.234 (0.901)	0.147 (0.724)
Emo Con	FvH	R	Amyg	F = 0.077, p = 0.781	F = 0.378, p = 0.540	-0.157 (1.060)	-0.173 (1.134)	-0.125 (1.077)	-0.318 (1.010)
Emo Con	FvH	L	Amyg	F = 0.390, p = 0.533	F = 0.020, p = 0.887	-0.330 (0.830)	-0.195 (1.000)	-0.164 (1.345)	-0.120 (1.134)
Emo Con	iI-cI	L	Ant Ins	F = 2.259, p = 0.136	F = 0.250, p = 0.618	-0.172 (0.604)	-0.179 (0.359)	-0.077 (0.326)	-0.011 (0.399)
Emo Con	iI-cI	R	Ant Ins	F = 3.059, p = 0.083	F = 0.095, p = 0.758	-0.181 (0.506)	-0.174 (0.420)	-0.048 (0.415)	-0.008 (0.424)
Emo Con	iI-cI	R	Amyg	F = 0.073, p = 0.787	F = 0.014, p = 0.906	-0.085 (0.528)	-0.148 (0.375)	-0.075 (0.470)	-0.093 (0.760)
Emo Con	iI-cI	L	Amyg	F = 0.176, p = 0.676	F = 0.703, p = 0.404	-0.040 (0.514)	-0.011 (0.453)	0.070 (0.502)	-0.047 (0.447)
Reap	LNeg-Neut	L	Ant Ins	F = 0.068, p = 0.796	F = 0.449, p = 0.504	0.032 (0.098)	0.013 (0.078)	0.035 (0.058)	0.018 (0.080)
Reap	LNeg-Neut	R	Ant Ins	F = 0.631, p = 0.430	F = 0.285, p = 0.594	0.011 (0.092)	-0.002 (0.087)	0.026 (0.073)	0.011 (0.101)
Reap	LNeg-Neut	R	Amyg	F = 0.886, p = 0.352	F = 0.264, p = 0.608	0.037 (0.105)	-0.041 (0.102)	0.028 (0.061)	0.002 (0.108)
Reap	LNeg-Neut	L	Amyg	F = 0.195, p = 0.661	F = 0.867, p = 0.354	0.044 (0.100)	-0.025 (0.114)	0.016 (0.054)	-0.012 (0.100)
Reap	Reap-LNeg	L	Ant Ins	F = 1.381, p = 0.243	F = 2.044, p = 0.156	-0.003 (0.112)	0.035 (0.135)	0.013 (0.092)	-0.036 (0.107)
Reap	Reap-LNeg	R	Ant Ins	F = 1.355, p = 0.247	F = 2.284, p = 0.134	0.019 (0.122)	0.037 (0.144)	0.027 (0.120)	-0.030 (0.107)
Reap	Reap-LNeg	R	Amyg	F = 1.423, p = 0.236	F = 0.000, p = 0.990	-0.001 (0.085)	0.024 (0.125)	-0.014 (0.086)	-0.015 (0.138)
Reap	Reap-LNeg	L	Amyg	F = 0.342, p = 0.560	F = 0.510, p = 0.477	-0.012 (0.089)	0.006 (0.151)	-0.004 (0.112)	-0.030 (0.126)

*Task column specifies the functional task, while the contrast column specifies the contrast of task conditions; Time Effect column and Ttreatment Arm x Time Effect Colum specify the statistics from a linear mixed model analysis testing for differential change in each region of interest; * denotes an effect is*

significant at p < 0.05; Emo Con = emotional conflict task; Emo Reac = emotional reactivity task; F-N = conscious (unmasked) fear vs. neutral faces; FvH = congruent fear vs. congruent happy trials; iI-cI = conflict regulation (post-incongruent incongruent trials vs. post-congruent incongruent trials); Inc-Con = incongruent vs. congruent trials; L = left; LNeg-Neut = look negative vs. look neutral trials; MF-MN = nonconscious (masked) fear vs. neutral faces; MNI = Montreal Neurological Institute; R = right; Reap = reappraisal task; Reap-LNeg = reappraise negative vs. look negative trials; ROI = region of interest; WB = whole brain.

TABLE S6. Differential Activation Changes by Treatment Arm During Reappraisal

Mask	Hem.	MNI Atlas Region(s)	# Voxels	X	Y	Z	Voxel Stats		Extractions		Predicted Activation (mean, SD)			
							FDR Z		*Parameter, Significance*		Pre		Post	
							Mean	*SD*	*PE*	*WL*	PE	WL	PE	WL
Reappraise Negative vs. Look Negative														
ROI	L	Middle Frontal Gyrus	60	-24	52	6	2.67	0.020	0.17, 0.002	-0.06, 0.22	0.00, 0.07	0.02, 0.05	0.12, 0.08	-0.03, 0.04

X, Y, and Z values are cluster center of mass coordinates in MNI stereotactic space; Voxel stats column depicts the mean and standard deviation of the voxelwise statistics for each clustered effect; Extractions column reports the mixed model parameter and significance value using extracted individual cluster beta values for each subject, specifying the slope of activation change within each treatment arm; Predicted activation column lists the summary statistics (mean and standard deviation) by group and time point for each individual's predicted level of activation derived from the mixed model; FDR = false discovery rate; Hem = hemisphere; L = left; MNI = Montreal Neurological Institute; PE = prolonged exposure treatment group; R = right; ROI = regions of interest; Sig. = significance; WB = whole brain exploratory analysis; WL = waitlist group.

TABLE S7. Differential Left Frontopolar Connectivity Changes by Treatment Arm During Reappraisal

Mask	Hem.	MNI Atlas Region(s)	# Voxels	X	Y	Z	Voxel Stats		Extractions		Predicted Connectivity (mean, SD)			
							FDR Z		*Parameter, Significance*		Pre		Post	
							Mean	*SD*	*PE*	*WL*	PE	WL	PE	WL
Reappraise Negative vs. Look Negative														
ROI	L/R	Olfactory Cortex/Caudate Nucleus/Nucleus Accumbens/Anterior Cingulate/Mid-Orbital Gyrus	200	0	23	-6	1.98	0.007	0.23, 0.003	-0.13, 0.087	-0.01, 0.06	-0.01, 0.07	0.13, 0.09	-0.04, 0.08

X, Y, and Z values are cluster center of mass coordinates in MNI stereotactic space; Voxel stats column depicts the mean and standard deviation of the voxelwise statistics for each clustered effect; Extractions column reports the mixed model parameter and significance value using extracted individual cluster beta values for each subject, specifying the slope of connectivity change within each treatment arm; Predicted connectivity column lists the summary statistics (mean and standard deviation) by group and time point for each individual's predicted level of connectivity derived from the mixed model; FDR = false discovery rate; Hem = hemisphere; L = left; MNI = Montreal Neurological Institute; PE = prolonged exposure treatment group; R = right; ROI = regions of interest; Sig. = significance; WB = whole brain exploratory analysis; WL = waitlist group.

TABLE S8. Effects of Single Pulse TMS to the Left Frontopolar Cortex vs. Right Motor Cortex on BOLD Signal in Healthy Individuals

Mask	Hem.	MNI Atlas Region(s)	# Voxels	X	Y	Z	Voxel Stats		Extractions	
							Corrected Pval		*One Sample T-test Pval*	
							Mean	*SD*	*LFp*	*RM1*
Left Frontopolar Cortex vs. Right Motor Cortex Stimulation										
gPPI	L/R	Caudate Nucleus/Nucleus Accumbens/Anterior Cingulate/Olfactory Cortex	99	5	20	-7	0.016	0.009	<0.001	0.46
WB	L	Calcarine Gyrus/Lingual Gyrus	14	-11	-58	7	0.020	0.012	0.002	0.021

X, Y, and Z values are cluster center of mass coordinates in MNI stereotactic space; Voxel stats column depicts the mean and standard deviation of the voxelwise statistics for the corrected p value from the permutation test; Extractions column reports the significance value for a one sample t-test for each stimulation condition, using extracted individual cluster beta values for each subject; gPPI = ventromedial prefrontal/ventral striatal region of interest mask derived from the generalized psychophysiological interaction analysis in PTSD participants; Hem = hemisphere; L = left; LFp = left frontopolar cortex; MNI = Montreal Neurological Institute; Pval = p value; R = right; RM1 = right primary motor cortex; SD = standard deviation; Sig. = significance; WB = whole brain exploratory analysis.